Astronomy & Astrophysics manuscript no. artikkeli2
October 13, 2014
©ESO 2014

Statistical multifrequency study of narrow-line Seyfert 1 galaxies ⋆

E. Järvelä[1,2⋆⋆], A. Lähteenmäki[1,2], and J. León-Tavares[3,4]

[1] Aalto University Metsähovi Radio Observatory, Metsähovintie 114, Kylmälä, 02540, Finland
[2] Aalto University Department of Radio Science and Engineering, 13000, FI-00076 AALTO, Finland
[3] Instituto Nacional de Astrofísica Óptica y Electrónica (INAOE), Apartado Postal 51 y 216, 72000 Puebla, México
[4] Finnish Centre for Astronomy with ESO (FINCA), University of Turku,Väisäläntie 20, FI-21500 Piikkiö, Finland

Received ; accepted

arXiv:1410.2743v1 [astro-ph.GA] 10 Oct 2014

ABSTRACT

Context. High-energy γ-rays, which are produced by powerful relativistic jets, are usually associated with blazars and radio galaxies. In the current active galactic nuclei (AGN) paradigm, such jets are almost exclusively launched from massive elliptical galaxies. Recently, however, *Fermi*/LAT detected γ-rays from a few narrow-line Seyfert 1 galaxies and thus confirmed the presence of relativistic jets in them. Since NLS1 galaxies are assumed to be young evolving AGN, they offer a unique opportunity to study the production of relativistic jets in late-type galaxies.
Aims. Our aim is to estimate by which processes the emission of various kinds is produced in NLS1 galaxies and to study how emission properties are connected to other intrinsic AGN properties.
Methods. We have compiled the so far largest multiwavelength database of NLS1 sources. This allowed us to explore correlations between different wavebands and source properties using, for example, Pearson and Spearman correlations and principal component analysis. We did this separately for radio-loud and radio-quiet sources.
Results. Multiwavelength correlations suggest that radio-loud sources host relativistic jets that are the predominant sources of radio, optical, and X-ray emission. The origin of infrared emission remains unclear. Radio-quiet sources do not host a jet, or the jet is very weak. In them, radio and infrared emission is more likely generated via star formation processes, and the optical and X-ray emission originate in the inner parts of the AGN. We also find that the black hole mass correlates significantly with radio loudness, which suggests that NLS1 galaxies with more massive black holes are more likely to be able to launch powerful relativistic jets.

Key words. galaxies: active – galaxies: Seyfert – galaxies: statistics – X-rays: galaxies

1. Introduction

Narrow-line Seyfert 1 galaxies (NLS1) are a subclass of Seyfert galaxies first described in 1985 by Osterbrock & Pogge (1985). They are mostly hosted by spiral galaxies; however, a few of them are found in peculiar, interacting, or E/S0 systems (Ohta et al. 2007). Optical studies suggest that the disk-like host galaxies of NLS1 galaxies are more often barred (85 ± 7 %) than are the disk-like hosts of broad-line Seyfert 1 galaxies (BLS1) (40 - 70 %) (Ohta et al. 2007).

NLS1 galaxies are believed to be rather young active galactic nuclei (AGN) in the early stages of their evolution (Mathur et al. 2001). They harbor low- or intermediate-mass black holes ($M_{\rm BH} < 10^8\ M_\odot$) (Peterson et al. 2000) accreting at high rates (0.1-1 Eddington rate or even above) (Boroson & Green 1992) and tend to lie below the normal $M_{\rm BH} - \sigma_*$ (stellar velocity dispersion of the bulge) and $M_{\rm BH} - L_{\rm bulge}$ (luminosity of the bulge) relations (Mathur et al. 2001), suggesting that they are still evolving. Radio-quiet NLS1 galaxies also show enhanced star formation (Sani et al. 2010).

In NLS1 galaxies permitted emission lines are narrow, making them of comparable width with narrow forbidden lines. Characterizing spectral features are FWHM(Hβ) < 2000 km s^{-1} (Goodrich 1989) and [O III]/Hβ < 3 (with exceptions allowed if there are strong [Fe VIII] and [Fe X] present) (Osterbrock & Pogge 1985). Some but not all NLS1 sources show strong Fe II emission (Osterbrock & Pogge 1985).

NLS1 sources show a strong soft X-ray excess, and some of them also exhibit very rapid, high-amplitude variability at X-rays. Overall they have more diverse soft X-ray (0.1-2.5 keV) photon indices ($\Gamma \approx 1$ - 5) than Type 1 Seyfert galaxies ($\Gamma \approx 2$) (Boller et al. 1996). There is a relation between FWHM(Hβ) and the X-ray spectral slope $\alpha_{\rm X}$. Sources with narrower Hβ tend to have steeper X-ray spectra (Puchnarewicz et al. 1992; Boller et al. 1996).

NLS1 sources are generally radio-quiet, but studies have shown that ∼7% of them are radio-loud (Komossa et al. 2006). However, they generally have a very compact radio morphology; evidence of large scale structures has been found only in six NLS1 sources (Gliozzi et al. 2010; Doi et al. 2012). All of these sources are radio-loud and have on average more massive black holes than the NLS1 population in general. Five of six sources have $M_{\rm BH} > 10^7 M_\odot$ (Doi et al. 2012).

The spectral energy distributions (SEDs) of some radio-loud NLS1 sources are similar to the SEDs of blazars. In them the most prominent features are two broad components, one extending from radio to soft X-rays and the other covering hard X-rays and γ-rays. The first bump is believed to be due to synchrotron emission and the second bump due to inverse-Compton (IC) scattering.

Although some NLS1 galaxies show blazar-like behavior, no γ-ray emission was expected due to their host galaxy type.

⋆ Tables 1, 2, 5, 7, 8, 12, and 13, and Figures 2, 4, 5, and 7 are only available in electronic form via http://www.edpsciences.org
⋆⋆ e-mail: emilia.jarvela@aalto.fi

That changed in 2008 when the Large Area Telescope[1] onboard *Fermi Gamma-ray Space Telescope*[2] (hereafter *Fermi*) detected γ-ray emission from the source PMN J0948+0022 identified as a NLS1 galaxy (Abdo et al. 2009a). Consequently two multiwavelength campaigns were launched to better understand its nature. During the first campaign (March-July 2009) it was confirmed that the γ-ray emission is indeed associated with the known radio-loud NLS1 PMN J0948+0022 (Abdo et al. 2009b; Yuan et al. 2008). Later, during the second multiwavelength campaign (July-September 2010) it flared at γ-rays and reached the extreme power of $\sim 10^{48}$ erg s^{-1} in the 0.1-100 GeV band (Foschini et al. 2011).

So far five NLS1 sources have been detected with high significance at γ-rays confirming that they are a new class of γ-ray emitting AGN, in addition to blazars and radio galaxies. The discovery of γ-ray emission from NLS1 galaxies was remarkable because in the current AGN paradigm powerful relativistic jets are almost exclusively launched from massive elliptical galaxies with supermassive black holes (Urry 2003). Blazars and radio galaxies, and NLS1 galaxies have different hosts (late-type in NLS1 galaxies), $M_{\rm BH}$ (smaller in NLS1 galaxies), accretion rates (higher in NLS1 galaxies), and radio morphologies (compact in NLS1 galaxies). Yet we now know that NLS1 galaxies can form and launch a fully developed relativistic jet. This poses many interesting questions concerning AGN and relativistic jet evolution, and challenges our current knowledge of jet systems. Therefore, NLS1 galaxies offer a great opportunity to study the evolution of relativistic jets and further our understanding about the mechanisms that drive AGN activity.

In this study our aim is to estimate via which processes and, if possible, where the various kinds of emission are produced in NLS1 galaxies. We address this issue by compiling multiwavelength observations from literature for a large sample of NLS1 sources. This allows us to explore correlations between different wavebands, and identify the most likely radiation mechanism responsible for the bulk of the energy released in NLS1 sources. We are also interested in how the emission properties are connected with other intrinsic AGN properties, for example, the black hole mass.

Throughout the paper we assume a cosmology with $H_0 = 73$ km s^{-1} Mpc^{-1}, $\Omega_{\rm matter} = 0.27$ and $\Omega_{\rm vacuum} = 0.73$.

2. Sample selection

Our sample was selected using three references: Zhou et al. (2006), Yuan et al. (2008), and Komossa et al. (2006). The original sample in Zhou et al. (2006) consists of 2011 NLS1 sources selected from Sloan Digital Sky Survey[3] (SDSS) Data Release 3 with restrictions $z \lesssim 0.8$ and the 'broad' component of Hβ or Hα narrower than 2200 km s^{-1} at the 10 σ or higher confidence level. From this sample, using ASI Science Data Center's (ASDC[4]) Sky Explorer and SED Builder, we selected sources which had radio data from the Very Large Array (VLA) Faint Images of the Radio Sky at Twenty-Centimeters (FIRST[5]) survey. This makes a total of 280 sources which we included in our sample.

The sample in Yuan et al. (2008) consists of 23 radio-loud NLS1 sources selected from SDSS Data Release 5 under the same restrictions as in Zhou et al. (2006). 12 of them overlap with the Zhou et al. (2006) sample; we included the remaining 11 new sources to our sample.

Our third reference Komossa et al. (2006) has a sample of 11 radio-loud NLS1 sources found by cross-correlating the Catalogue of Quasars and Active Nuclei (Veron-Cetty & Veron 2003) with several radio and optical catalogs using the cross-matcher application developed within the German Astrophysical Virtual Observatory (GAVO)[6] project. The sample was limited by the requirement Hβ < 2000 km s^{-1}. From Komossa et al. (2006) we were able to include only one source to our sample since some of them overlapped sources from Zhou et al. (2006) and Yuan et al. (2008), and some of them did not have radio data. Our final sample consists of 292 NLS1 galaxies.

All the data for our sample were gathered from publicly available archival sources, and it should be noted that they are therefore not simultaneous. Studying correlations between wavebands of variable sources, such as AGN, should ideally be performed with data that are no more than a couple of weeks apart, but in practise this is often impossible. Radio data from FIRST, optical data from SDSS, and X-ray data from ROSAT[7] All Sky Survey (RASS) were retrieved from ASDC. We have radio and optical data for all of our sources, and X-ray data for 109 sources (hereafter called the X-ray sample). Data obtained from ASDC were already corrected for galactic extinction.

Infrared data from Wide-field Infrared Survey Explorer (WISE[8]) All-Sky Source Catalog[9] (Cutri & et al. 2012) were retrieved from the NASA/IPAC Infrared Science Archive (IRSA[10]). We used a search radius of 2.″4 (Massaro et al. 2011) and a minimum signal-to-noise ratio >7 in at least one band. We found a match for 291 sources. Nine sources were excluded from the sample due to the contamination risk[11], thus we have infrared data for 282 sources. Infrared data are not corrected for the galactic absorption because the correction would be smaller than the uncertainties in magnitudes. Flux densities (in Janskys) were computed using the WISE magnitudes[12].

Additional W4-band correction suggested by the WISE Explanatory Supplement was done for 'red' sources with $\alpha > 1$ (α being power-law index: $F_\nu \propto \nu^{-\alpha}$). α was estimated using [W1-W2] and [W2-W3] colors and a table in Wright et al. (2010). Corrections were computed with the equation: F_ν [W4] = 0.9 × F_ν [W4]. Flux densities for all of our sources are listed in Online Table 1.

Luminosities for all wavebands were computed from the equation

$$L = 4\pi D_{\rm L}^2 \nu F_\nu \quad (1)$$

where $D_{\rm L}$ is the luminosity distance to the source and F_ν flux density in Janskys. $D_{\rm L}$ values were obtained from the NASA/IPAC Extragalactic Database[13] (NED).

[1] http://fermi.gsfc.nasa.gov/science/instruments/lat.html
[2] http://fermi.gsfc.nasa.gov/
[3] www.sdss.org
[4] www.asdc.asi.it
[5] www.sundog.stsci.edu
[6] www.g-vo.org
[7] http://heasarc.gsfc.nasa.gov/docs/rosat/rosgof.html
[8] www.nasa.gov/wise
[9] http://wise2.ipac.caltech.edu/docs/release/allsky/
[10] http://www.irsa.ipac.caltech.edu
[11] For sources with non-zero cc_flags -column it is adviced in the WISE Explanatory Supplement that the observation should be ignored because one or more bands might be somehow contaminated.
[12] http://wise2.ipac.caltech.edu/docs/release/allsky/expsup/sec4_4h.html
[13] www.http://ned.ipac.caltech.edu/

3. Data analysis

3.1. Radio-loudness

We computed radio loudness (*RL*) for all of our sources. We used the commonly defined *RL* value; the ratio of 1.4 GHz radio flux density (F_R) and 440 nm optical flux density (F_O). For F_R we used the K-corrected (we did K-correction as suggested in Foschini (2011)) radio flux density from the FIRST survey and for F_O the K-corrected B-band optical flux density calculated using SDSS *u*- and *g*-band magnitudes[14,15]. The radio loudness values for our sources are listed in Online Table 2.

We then divided the sources to four subsamples by their radio loudness. The subsamples are: radio-quiet (RQ; $RL < 10$, 97 sources), radio-loud (RL; $RL > 10$, 195 sources), very radio-loud (VRL; $RL > 100$, 51 sources), and super radio-loud (SRL; $RL > 1000$, 10 sources). The radio-loud subsample includes very radio-loud and super radio-loud subsamples. The subsamples and their sizes by waveband are presented in Table 3.

3.2. Parent population

We used the two-sample Kolmogorov-Smirnov test (hereafter K-S test) with 5% significance level (probability value p<0.05) in order to examine whether the parent population of our radio-quiet and radio-loud subsamples is the same.

Mean redshifts and standard deviations for the different subsamples are given in Table 3. The K-S test for redshift suggests that our radio-quiet and radio-loud subsamples are not originally from the same distribution ($p=1.42\times10^{-4}$). The distributions are shown in Figure 1. In our sample, radio-quiet sources tend to lie closer than radio-loud sources.

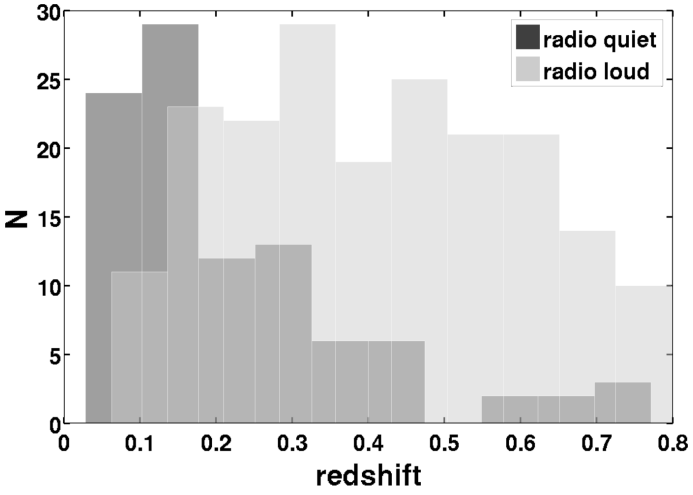

Fig. 1: Redshift distributions of the radio-quiet and radio-loud subsamples.

The K-S test also suggests that radio-quiet and radio-loud subsamples are not drawn from the same luminosity distribution. P-values for the K-S test are small, from 0.013 to $\sim 10^{-26}$. Radio-loud sources are on average more luminous than radio-quiet sources. This holds for all wavebands. Examples of radio-loud and radio-quiet luminosity distributions are shown in Online Figure 2.

[14] http://www.sdss.org/dr5/algorithms/sdssUBVRITransform.html
[15] http://www.sdss.org/dr5/algorithms/fluxcal.html#sdss2ab

3.2.1. Black hole mass estimation

There are three methods commonly used to estimate the black hole mass (M_{BH}) in AGN. These methods make use of the stellar velocity dispersion of the bulges (σ_*), the mass of the bulge (M_{bulge}, Bentz et al. (2009)), and FWHM(Hβ) or FWHM(Hα). We calculated M_{BH} estimations using the FWHM(Hβ) – luminosity mass scaling relation (see Greene & Ho (2005) for more details)

$$M_{BH} = (4.4\pm0.2)\times10^6\left(\frac{L_{5100}}{10^{44}\ \mathrm{ergs\ s^{-1}}}\right)^{0.64\pm0.02}\left(\frac{\mathrm{FWHM}(H\beta)}{10^3\ \mathrm{km\ s^{-1}}}\right)^2 M_\odot \quad (2)$$

where L_{5100} is the monochromatic luminosity at 5100Å. L_{5100} and FWHM(Hβ) values were taken from Zhou et al. (2006). We used this method because there is no comprehensive enough information about σ_* or L_{bulge} for our sources. However, it does not take into account possible inclination effects caused by the geometry of the broad-line region (BLR) of the source and the viewing angle (Decarli et al. 2011). NLS1 sources also tend to lie below the normal $M_{BH}-\sigma_*$ and $M_{BH}-L_{bulge}$ relations (Mathur et al. 2001; Laor 2001).

We were able to estimate the M_{BH} for 275 sources. The mean values and standard deviations are shown in Table 3, and the black hole mass estimates for individual sources are listed in Online Table 2.

The K-S test for M_{BH} suggests that the radio-quiet and radio-loud subsamples are not drawn from the same distribution ($p=2.04\times10^{-4}$). On average radio-loud sources have more massive black holes than radio-quiet sources. McLure & Jarvis (2004) got similar results for a large sample of quasars (6099 radio-quiet and 436 radio-loud sources). The M_{BH} distributions of the radio-loud and radio-quiet subsamples are shown in Figure 3.

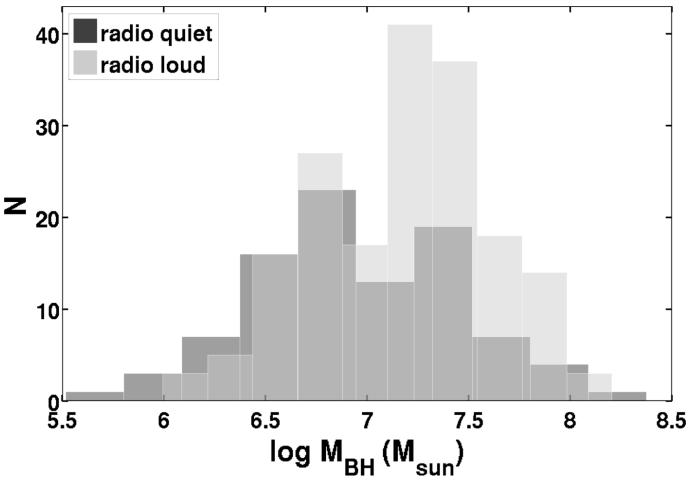

Fig. 3: Black hole mass distribution of the radio-quiet and radio-loud subsamples.

3.3. Multiwavelength correlations

Results of multiwavelength correlations in literature are diverse and especially for NLS1 sources also very sparse. Arshakian et al. (2010) found $L_{R,\,total} - L_O$ correlation for a sample of ~100 quasars, and $L_{R,\,jet} - L_O$ correlation for BL Lac objects (~18).

Table 3: Sample sizes at different wavebands, mean redshifts and their standard deviations (std), and mean black hole masses and their standard deviations for the whole sample and the subsamples.

sample	N	N_R	N_{IR}	N_O	N_X	N_{IR} and N_X	z		$\log M_{BH}(M_\odot)$	
							mean	std	mean	std
all	292	292	282	292	109	105	0.35	0.20	7.10	0.47
RQ	97	97	90	97	60	56	0.22	0.17	6.96	0.52
RL	195	195	192	195	49	49	0.41	0.19	7.18	0.43
VRL	51	51	51	51	16	16	0.48	0.17	7.31	0.39
SRL	10	10	10	10	4	4	0.54	0.17	7.30	0.40

Ballo et al. (2012) concluded that in a sample of 852 quasars and 14 Seyfert galaxies there is $L_R - L_X$ correlation but no $L_O - L_X$ correlation, whereas Brinkmann et al. (2000) found a correlation for both in a mixed sample. $L_R - L_X$ correlation has also been found in several other studies (Younes et al. (2012) for six LINER 1 sources, Panessa et al. (2007) for 47 Seyfert galaxies and 33 low-luminosity radio galaxies, Bianchi et al. (2009) for 156 radio-quiet X-ray unobscured AGN). Connection between radio and gamma-ray emission in radio-loud AGN has been confirmed by, for example, Jorstad et al. (2001), Lähteenmäki & Valtaoja (2003) and Nieppola et al. (2011), and between mm and submm and gamma-ray emission by León-Tavares et al. (2012).

We used Pearson product-moment correlation coefficient (Pearson's r), Spearman's rank correlation coefficient (Spearman's ρ) and Pearson and Spearman partial correlation coefficients to study how the different wavebands are connected. The correlation is significant and the null hypothesis rejected if $p<0.05$.

We computed correlations for the flux densities for the whole sample and for all the subsamples individually. The correlations are shown in Table 4 and the most significant results are shown in Online Table 5. The flux densities used to calculate the results presented in Table 5 are the optical and radio flux densities used to calculate the radio-loudness, WISE W1 infrared flux density, and RASS X-ray flux density. We used SDSS g-band because it is closest to B-band which we used to calculate the radio-loudness. All the infrared and optical bands had very similar correlation results, therefore we present correlations for just one infrared and one optical band.

The same correlations were computed also for luminosities, and in addition we determined the Pearson's r and Spearman's ρ partial correlation coefficients for all the correlations shown in Table 4. For luminosities the used wavebands are FIRST, SDSS g-band, WISE W1-band, and RASS. The results are again presented for one infrared and one optical band due to the similarity of the results in all bands. For partial correlations we used redshift as the third parameter to rule out the possibility that the possible correlation is not real but caused by redshift. The main results for partial correlations are shown in Table 6 and L–L plots in Online Figure 4. All other calculated multiwavelength correlations, e.g., the other optical and infrared wavebands, all luminosity correlations, and correlations for the X-ray selected samples did not differ significantly from the results presented here so they are omitted.

In addition to flux density and luminosity correlations we studied correlations $M_{BH} - RL$, $M_{BH} - L$ (Table 12), and FWHM(Hβ) – L (Table 13). They are discussed in more detail in Sections 3.5, 3.6, and 3.7.

In order to get more insight into whether the origin of the emission at certain wavebands is the same in our radio-quiet and radio-loud subsamples, we computed linear fits (y = ax + b) for flux densities and luminosities between different wavebands by using the least squares method. Totally distinct slopes would suggest a different origin. Results for the fits for flux densities are shown in Online Table 7 and for luminosities in Online Table 8.

The multiwavelength correlations and linear fits are discussed in the next section.

3.3.1. Radio-loud and radio-quiet sources

The results for flux density, luminosity, and partial luminosity correlations were similar.

In the radio-loud subsample the optical band correlates rather well with the infrared (all subsamples) and X-ray (RL sample as a whole but not for VRL and SRL subsamples separately) bands. The correlation between the optical and radio bands becomes obvious only when looking at the VRL and SRL subsamples. This suggests that in radio-loud sources radio, optical, and at least partially also X-ray emission come mostly from the jet as the jet emits low-energy synchrotron radiation (radio emission) and high-energy IC emission (X-ray emission). However, a portion of the X-ray emission might also originate in the hot corona of the accretion disk via IC. Similarly, optical emission is supposedly composed of non-thermal emission from the jet and thermal emission from the accretion disk. Radio and infrared emission do not correlate (except for the SRL subsample which, however, is very small and therefore the correlation cannot be considered convincing) which might indicate that infrared emission is rather of thermal than non-thermal origin, for example, from the dusty torus (reprocessed emission from the accretion disk) or from star formation (reradiated starlight) (Bressan et al. 2006). Radio emission does not correlate with X-rays either. This is probably due to the very high and rapid X-ray variability exhibited by NLS1 sources (e.g. Leighly (1999); Komossa & Meerschweinchen (2000)). X-ray emission is variable in very short time scales, and since we have only one X-ray waveband observation per source, the observed X-ray flux value is highly coincidental. We also do not have any simultaneous radio and X-ray data.

In the radio-quiet subsample the optical band correlates very well with the infrared, and moderately well with radio and X-ray bands. Due to the radio-quietness of these sources it is likely that they do not host a jet or the jet is not powerful enough to dominate the emission. The predominant source of radio emission in the radio-quiet subsample could therefore be supernova remnants (Condon 1992). In fact, radio emission does not correlate too well with the X-ray emission which probably is produced in the hot corona of the accretion disk via IC. As for the optical emission, it probably comes from the accretion disk. Radio and infrared bands correlate moderately well which suggests that infrared emission is generated by star formation as reradiated starlight (Botticella et al. 2012). However, dust heated by

the AGN should also be taken into account when modeling both radio-quiet and radio-loud AGN (Mason et al. 2013).

Linear fits for flux densities and luminosities show very different slopes for the radio-quiet and radio-loud subsamples. For example, $S_{\rm IR} - S_{\rm R}$ slope for the radio-quiet subsample is 0.759, whereas for the radio-loud it is 0.070. Corresponding slopes for luminosities are 0.754 and 0.373. This suggests that the infrared emission mechanism is different for the radio-quiet and radio-loud sources.

Table 4: Flux density and luminosity correlations between the different wavebands.

	FIRST	SDSS g	RASS
FIRST	-	r, ρ, r_x, ρ_x	r_x, ρ_x
SDSS $u/g/r/i/z$	r^a , ρ^b , $r_x{}^c$, $\rho_x{}^d$	-	r_x, ρ_x
WISE W1–4	r, ρ, r_x, ρ_x	r, ρ, r_x, ρ_x	r_x, ρ_x
RASS	r_x, ρ_x	r_x, ρ_x	-

Notes. [(a)] Pearson's r [(b)] Spearman's ρ [(c)] Pearson's r for X-ray sample [(d)] Spearman's ρ for X-ray sample

3.4. Principal component and cluster analysis

Principal component analysis (PCA) is a statistical method used to simplify large amounts of data. It converts a set of possibly correlated variables into a set of uncorrelated variables called principal components, or eigenvectors. The first principal component accounts for as much of the variability in the data as possible. The second principal component has as large a variance as possible while still being orthogonal to the first principal component, and so on. This method makes it possible to find underlying connections and the most dominant variables in a data set, and possibly helps to identify the physical properties connected with each eigenvector. A good overview of the PCA in astronomy can be found in Francis & Wills (1999).

Boroson & Green (1992) used PCA to study the optical properties of 87 quasi-stellar objects (QSO). In their study Eigenvector 1 (EV1) is dominated by the anticorrelation between the strength of Fe II, and the strength of [OIII] λ5007 and FWHM(Hβ), and Eigenvector 2 (EV2) distinguishes between the strength of He II λ4686 and optical luminosity. This study was continued in Boroson (2002) where 75 sources were added to the original sample. The results for the first two principal components were similar to the earlier study. They suggest that EV1 corresponds closely to the Eddington ratio, $L/L_{\rm Edd}$, and EV2 to the accretion rate. Xu et al. (2012) studied a sample of narrow-line and broad-line Seyfert 1 galaxies using PCA. Their results were consistent with Boroson & Green (1992) and Boroson (2002). In a study of 110 soft X-ray -selected AGN, of which about half were NLS1 galaxies, Grupe (2004) found the EV1 to be similar to the EV1 in Boroson (2002). EV2 in their study correlated strongly with the black hole mass.

We performed weighted principal component analysis (PCA) using the pca[16] function in MATLAB Statistics Toolbox for the whole sample (97 sources), the radio-loud subsample (41 sources), the radio-quiet subsample (56 sources), and the corresponding modified samples (super radio-loud outlier, SDSS J104732.68+472532.1, removed). We carried out PCA with seven variables for all samples. The variables used were the radio flux density (FIRST), infrared flux density (WISE W1-band), optical flux density (SDSS g-band), X-ray flux density (RASS), $M_{\rm BH}$, FWHM(Hβ) (Hβ broad component FWHM), and R4570 (optical Fe II strength relative to broad Hβ component). We included R4570 to the PCA because it is possibly related to the radio emission. For example, Yuan et al. (2008) found that the optical Fe II emission is on average stronger for radio-loud NLS1 sources than for the NLS1 population in general. Values for FWHM(Hβ) and R4570 were taken from Zhou et al. (2006). To start with, we tried several combinations of variables and, for example, correlated $M_{\rm BH}$, in the cases when it was left out of the PCA, with the Eigenvectors along the lines of Xu et al. (2012) and Grupe (2004). Unfortunately, most of these experiments did not yield any convincing results so instead we changed the focus of the analysis to how the different properties are linked to each other, and therefore decided to include $M_{\rm BH}$ in the PCA. This proved to be a more informative approach.

Results only for the first and the second principal components are presented because the results for the subsequent components were mixed and no conclusions could be drawn from them. The PCA coefficients are listed in Tables 9 and 10. In the tables, the coefficients have been grouped together based on their sign, i.e. whether they correlate or anticorrelate with the Eigenvector. In this way, it is easier to see which properties might be linked to each other.

We also tried cluster analysis for our whole sample in order to see if there are any distinguishable groups within our sample. We tried both hierarchical clustering and k-Means clustering with five variables: radio flux density (FIRST), infrared flux density (WISE W1-band), optical flux density (SDSS g-band), X-ray flux density (RASS), and $M_{\rm BH}$. Cluster analysis did not yield any compelling results.

Table 9: Results of the principal component analysis with seven variables, eigenvector 1. The coefficients have been grouped together based on their sign.

-	sample	+
IR -0.48 optical -0.52 X-ray -0.39	All (35%)	radio 0.20 log $M_{\rm BH}$ 0.45 FWHM(Hβ) 0.32 R4570 0.04
IR -0.50 optical -0.55 X-ray -0.41	All, modified (34%)	radio 0.10 log $M_{\rm BH}$ 0.44 FWHM(Hβ) 0.28 R4570 0.06
IR -0.53 optical -0.50 X-ray -0.16 R4570 -0.08	Radio-loud (37%)	radio 0.21 log $M_{\rm BH}$ 0.49 FWHM(Hβ) 0.39
radio -0.01 IR -0.57 optical -0.54 X-ray -0.15 R4570 -0.07	Radio-loud, modified (35%)	log $M_{\rm BH}$ 0.48 FWHM(Hβ) 0.36
radio -0.40 IR -0.48 optical -0.56 X-ray -0.35	Radio-quiet (37%)	log $M_{\rm BH}$ 0.35 FWHM(Hβ) 0.12 R4570 0.19

[16] http://www.mathworks.se/help/stats/pca.html

Table 6: Pearson's r and Spearman's ρ partial luminosity correlations and their p-values for the whole sample and the subsamples. Correlations in boldface have p<0.05

	$\log L_O$ - $\log L_R$		$\log L_O$ - $\log L_{IR}$		$\log L_O$ - $\log L_X$	
sample	Pearson's r (p)	Spearman's ρ (p)	r (p)	ρ (p)	r (p)	ρ (p)
all	0.033 (0.571)	-0.044 (0.457)	**0.701** ($\sim 10^{-43}$)	**0.699** ($\sim 10^{-42}$)	**0.484** ($\sim 10^{-7}$)	**0.456** ($\sim 10^{-7}$)
RQ	**0.507** ($\sim 10^{-7}$)	**0.528** ($\sim 10^{-8}$)	**0.767** ($\sim 10^{-18}$)	**0.734** ($\sim 10^{-16}$)	**0.476** ($\sim 10^{-4}$)	**0.384** (0.003)
RL	**0.223** (0.002)	**0.160** (0.026)	**0.607** ($\sim 10^{-20}$)	**0.575** ($\sim 10^{-18}$)	**0.538** ($\sim 10^{-5}$)	**0.451** (0.001)
VRL	**0.527** ($\sim 10^{-5}$)	**0.577**($\sim 10^{-5}$)	**0.448** (0.001)	**0.605** ($\sim 10^{-6}$)	0.422 (0.117)	0.233 (0.402)
SRL	**0.744** (0.021)	**0.699** (0.036)	**0.950** ($\sim 10^{-5}$)	**0.931** ($\sim 10^{-4}$)	0.505 (0.663)	-0.218 (0.860)

	$\log L_R$ - $\log L_{IR}$		$\log L_R$ - $\log L_X$	
sample	Pearson's r (p)	Spearman's ρ (p)	r (p)	ρ (p)
all	0.030 (0.613)	-0.078 (0.192)	0.151 (0.119)	0.184 (0.057)
RQ	**0.546** ($\sim 10^{-8}$)	**0.380** ($\sim 10^{-4}$)	0.230 (0.079)	**0.314** (0.016)
RL	0.101 (0.163)	0.018 (0.800)	0.201 (0.171)	0.277 (0.057)
VRL	0.094 (0.518)	0.269 (0.059)	0.218 (0.436)	0.310 (0.261)
SRL	**0.676** (0.048)	**0.806** (0.009)	0.171 (0.890)	N/A (N/A)

Table 10: Results of the principal component analysis with seven variables, eigenvector 2. The coefficients have been grouped together based on their sign.

-	sample	+
R4570 -0.52	All (22%)	radio 0.21 IR 0.31 optical 0.28 X-ray 0.14 log M_{BH} 0.28 FWHM(Hβ) 0.64
radio -0.02 R4570 -0.54	All, modified (22%)	IR 0.27 optical 0.23 X-ray 0.09 log M_{BH} 0.31 FWHM(Hβ) 0.69
X-ray -0.21 R4570 -0.56	Radio-loud (20%)	radio 0.29 IR 0.29 optical 0.41 log M_{BH} 0.001 FWHM(Hβ) 0.55
X-ray -0.23 log M_{BH} -0.06 R4570 -0.68	Radio-loud, modified (19%)	radio 0.04 IR 0.16 optical 0.32 FWHM(Hβ) 0.59
X-ray -0.06 R4570 -0.41	Radio-quiet (24%)	radio 0.11 IR 0.25 optical 0.06 log M_{BH} 0.48 FWHM(Hβ) 0.72

3.4.1. Eigenvector 1

EV1 accounts for 34% – 37% of the variance. In all samples and subsamples EV1 distinguishes between M_{BH} and both optical and infrared emissions. The latter two are always connected. X-ray emission behaves similarly to infrared and optical but contributes less. Radio emission is rather insignificant except in the radio-quiet subsample where it is connected with optical and infrared, confirming the suggestion that in the radio-quiet sources radio emission is rather of stellar origin. FWHM(Hβ) is strongly connected with M_{BH} except in the radio-quiet subsample where it is less significant. R4570 is rather insignificant in all samples.

In all cases for EV1 the optical and infrared wavebands seem to be tightly connected, and opposite to M_{BH} and FWHM(Hβ). In the radio-quiet subsample also radio emission is connected with optical and infrared. In all cases the X-ray band behaves similarly to infrared and optical. These results suggest that optical and infrared emission (and up to some extent X-ray emission) – and in radio-quiet sources also the radio emission – are either of thermal or stellar origin i.e. not generated in a jet. The significance of M_{BH} implies that EV1 might be similar to EV2 in Grupe (2004).

3.4.2. Eigenvector 2

19%-24% of the variance is explained by EV2. It clearly distinguishes between R4570 and FWHM(Hβ) in all samples. To some extent also infrared and optical seem to be connected to FWHM(Hβ). Since EV2 is dominated by the anticorrelation of R4570 and FWHM(Hβ) it is similar to EV1 found in Boroson & Green (1992); Boroson (2002) and Xu et al. (2012).

3.4.3. Eddington ratio and eigenvector interpretation

In order to get more insight into the connection between the Eigenvectors and the physical properties of our sources, we calculated the Spearman rank correlation coefficients between the Eigenvectors and the Eddington ratio (L_{bol} / L_{Edd}). To compute the Eddington ratio we used the estimations $L_{bol} = 9\lambda\ L_{5100}$ (Kaspi et al. 2000) and $L_{Edd} = 1.3{\times}10^{38}\ M_{BH}$ / $M_{\odot}$ (Xu et al. 2012). Logarithmic mean, minimum, and maximum values for the Eddington ratio are -0.13, -0.75 and 0.48, respectively. The correlation results are shown in Table 11 and Online Figure 5.

EV2 strongly correlates with the Eddington ratio, and the correlation seems to be slightly better for the radio-loud samples. Similarly, Xu et al. (2012) found a correlation between their EV1 and the Eddington ratio. We also tried PCA with five variables - without FWHM(Hβ) and R4570 - and interestingly found no correlation between EV2 and Eddington ratio. I t seems that the connection is generated by FWHM(Hβ) and R4570. This is

supported by the results that FWHM(Hβ) and R4570 correlate strongly with Eddington ratio. For FWHM(Hβ) – $L_{\rm bol}$ / $L_{\rm Edd}$ correlation ρ = -0.71 (p=$\sim 10^{-16}$), and for R4570 – $L_{\rm bol}$ / $L_{\rm Edd}$ correlation ρ = 0.63 (p=$\sim 10^{-12}$). A weak correlation between EV1 and the Eddington ratio exists only for the radio-quiet sample.

As Grupe (2004) also points out, each sample has its own eigenvectors that depend on the parameters used and their range. In the earlier studies mixed samples, or samples not including NLS1 galaxies at all, have been used whereas we have looked at a pure NLS1 sample. Particularly in Boroson (2002) and Xu et al. (2012) the distribution of NLS1 galaxies, and also other pure samples containing just one source type, with respect to the two eigenvectors seems rather different from the distribution of the whole sample; distribution along EV2 is emphasized in the NLS1 group. This might indicate that the properties that appear in EV1 of the mixed samples, emerge in EV2 of pure samples. This could, for example, be interpreted as a sequence of properties that change from one source type to another thus creating the EV1 in mixed samples, and which is transformed to a sequence of properties within a pure sample of just one source type but in a less significant role (EV2 of our NLS1 sample). EV1 of our NLS1 sample would then describe those properties that cause most of the differences within that source type only. We also tested our analysis by performing it with optical data only, as has been done in the earlier studies, in case our additional data at other wavelengths or the black hole mass might influence the result. Variables used were the SDSS g-band flux density, λL5100Å, F(Hβ), FWHM(Hβ), F([OIII]) and R4570. The values for additional optical variables were taken from Zhou et al. (2006). This, however, did not change our results.

Table 11: Spearman rank correlations and probability values (in parentheses) for Eigenvectors 1 and 2 from PCA with seven variables, and log $L/L_{\rm Edd}$ for all samples. Correlations in boldface have p<0.05

sample	EV	log $L_{\rm bol}$ / $L_{\rm Edd}$
All	EV1	-0.053 (0.605)
	EV2	**-0.699** (0)
All, modified sample	EV1	-0.015 (0.886)
	EV2	**-0.719** (0)
Radio-loud	EV1	-0.184(0.247)
	EV2	**-0.767** ($\sim 10^{-8}$)
Radio-loud, modified sample	EV1	-0.136 (0.401)
	EV2	**-0.816** ($\sim 10^{-9}$)
Radio-quiet	EV1	**0.301** (0.024)
	EV2	**-0.598** ($\sim 10^{-6}$)

3.5. M_{BH} – radio-loudness correlations

Whether the correlation $M_{\rm BH}$ – RL in AGN really exists has been widely studied. The results are contradictory. Some studies suggest that the correlation exists (e.g., Laor (2000); Lacy et al. (2001); McLure & Jarvis (2004); Metcalf & Magliocchetti (2006); Chiaberge & Marconi (2011); Castignani et al. (2013)) whereas others conclude that there is no correlation (Oshlack et al. 2002; Woo & Urry 2002b) or the correlation at least is not clear (Ho 2002; Woo & Urry 2002a). In a study of 47 NLS1 galaxies Whalen et al. (2006) found an anticorrelation between $M_{\rm BH}$ and RL.

We found that the black hole mass and the radio-loudness weakly correlate for the whole sample with Pearson's r = 0.244 (p =$\sim 10^{-5}$) and Spearman's ρ = 0.212 (p=$\sim 10^{-4}$). This indicates that NLS1 galaxies with more massive black holes are more likely to be able to lauch powerful relativistic jets and are therefore louder at radio frequencies.

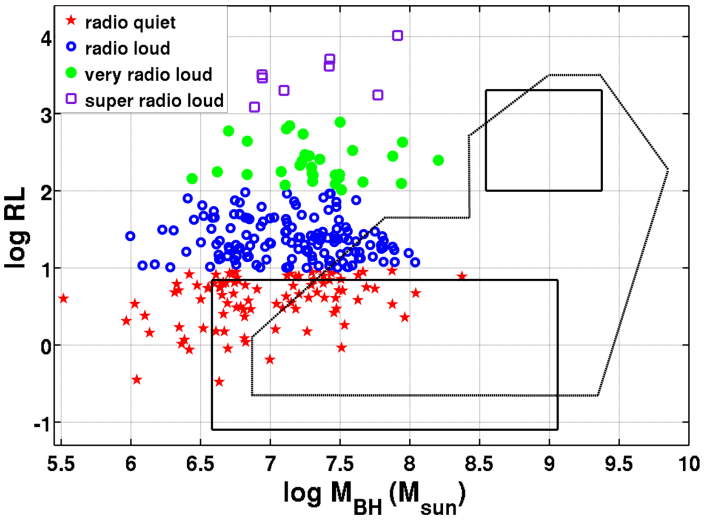

Fig. 6: Dependence of radio-loudness on black hole mass. Formerly populated regions from Komossa et al. (2006) shown with solid and dashed lines. Subsamples are shown with different symbols and colors; radio-quiet: filled red stars, radio-loud: open blue circles, very radio-loud: filled green circles, and super radio-loud: open purple squares.

Komossa et al. (2006) noticed that in the Laor diagram ($M_{\rm BH}$ – RL (Laor 2000)) NLS1 galaxies are located in a region formerly very sparsely populated with sources with rather small black hole masses (given their radio-loudness) compared to other AGN. We constructed a Laor diagram of our whole sample (Figure 6). Most of our sources also lie outside the formerly populated regions shown in Figure 4 in Komossa et al. (2006).

3.6. M_{BH} – luminosity correlations

Several previous studies have not shown $M_{\rm BH}$ – $L_{\rm R}$ correlation in AGN (e.g., Ho (2002); Woo & Urry (2002a); Oshlack et al. (2002); Snellen et al. (2003); Woo et al. (2005); León-Tavares et al. (2011); Park et al. (2013)). Woo et al. (2005) also studied the $M_{\rm BH}$ – $L_{\rm X}$ correlation (particularly in BL Lac objects) and did not find any support for it. In a study of radio-loud quasars Metcalf & Magliocchetti (2006) found no clear $M_{\rm BH}$ – $L_{\rm R}$ correlation but they did find a strong $M_{\rm BH}$ – $L_{\rm O}$ correlation. A large number of studies find a correlation between $M_{\rm BH}$ and $L_{\rm R}$ (e.g., McLure et al. (1999); Lacy et al. (2001); Dunlop et al. (2003); McLure & Jarvis (2004); Bianchi et al. (2009)). Bianchi et al. (2009) also found correlation between $M_{\rm BH}$ and $L_{\rm X}$.

We calculated the correlations using the FIRST, SDSS g-band, WISE W1-band, and RASS luminosities. The results are presented in Online Table 12 and $M_{\rm BH}$ – L plots in Online Figure 7. $M_{\rm BH}$ and luminosities at all wavebands correlate well for the whole sample and all subsamples; the correlation is strongest between $M_{\rm BH}$ and $L_{\rm O}$, and $M_{\rm BH}$ and $L_{\rm IR}$. This suggests that the more massive the black hole the more powerful the AGN. In radio-loud NLS1 sources, where most of the emission supposedly comes from the jet, this suggests that more massive black holes have more powerful jets. In radio-quiet sources, if radio emission comes from supernova remnants and infrared emission

from star formation, it is harder to explain why $M_{\rm BH}$ correlates with $L_{\rm R}$ and $L_{\rm IR}$.

3.7. FWHM(Hβ) – luminosity correlations

The wavebands used were the same as before. The results for the FWHM(Hβ) – L correlations for the whole sample and the subsamples are presented in Online Table 13. FWHM(Hβ) and luminosities in general correlate, although relatively weakly, for the whole sample and subsamples. Exception to this is the X-ray waveband which does not correlate with FWHM(Hβ). Also there does not seem to be any correlation among the very radio-loud and super radio-loud subsamples. This might be due to the very limited sizes of these samples. For the whole sample the strongest correlation is for FWHM(Hβ) – $L_{\rm O}$.

3.8. WISE blazar strip

Massaro et al. (2011) showed that WISE colors can be used to differentiate sources dominated by thermal or non-thermal emission on a [3.4]–[4.6]–[12] μm color diagram. Using a large sample of blazars they constructed the WISE γ-ray strip (WGS); a region populated by sources dominated by non-thermal emission. WGS makes it possible to identify new γ-ray emitters based on their WISE colors. We made use of this identification tool and constructed the WISE color diagram for our sources and for the whole Zhou et al. (2006) sample. We used the parametrizations presented in Massaro et al. (2012). They provided parameters for two partly overlapping strips; one for BL Lac objects and another for flat spectrum radio quasars (FSRQs).

The WISE color diagram constructed for our sample, WGS, and approximate regions populated by other types of sources (ultra luminous infrared galaxies, ULIRGs; luminous infrared galaxies, LIRGs; low-ionization nuclear emission-line region galaxies, LINERs) are shown in Figure 8. 72.7% of all, 57.8% of radio-quiet and 79.7% of radio-loud sources are located inside the WGS. The properties (e.g., radio-loudness, flux densities, luminosities, and $M_{\rm BH}$) for these sources are average compared to the whole sample. This suggests that infrared emission is of non-thermal origin and that most of our sources should host a jet. Some of our results are contradictory to this (see ***On the origin of infrared emission*** in Section 4). We expected that the difference between radio-quiet and radio-loud sources would be bigger since radio-loud sources should host a jet whereas radio-quiet should not. The reason for so many radio-quiet sources lying inside the WGS is unclear, but there are a few possible explanations. It might be that for some, yet unclear reason WGS does not apply for NLS1 galaxies. This might be due to the enhanced star formation in the circumnuclear regions of NLS1 galaxies because the star formation process is 'boosting' the infrared colors. Another possibility is that these sources really host a jet, but it is not powerful enough to dominate the whole electromagnetic spectrum.

1348 out of 1943 WISE detected sources from Zhou et al. (2006) lie inside the WGS. This is nearly the same percentage (69.4%) as in our sample which indicates that our sample represents the whole sample well.

4. Discussion

On the origin of infrared emission. Linear slope fitting suggests that infrared emission from radio-quiet and radio-loud sources has a different origin, supposedly thermal in radio-quiet and non-thermal in radio-loud sources. Multiwavelength correlations indicate that infrared emission in radio-quiet sources might be thermal whereas WGS indicates that it is non-thermal. The WGS also suggests that the origin in radio-loud sources is non-thermal. On the other hand the multiwavelength correlation results for radio-loud sources suggest that infrared emission is of thermal origin. Principal component analysis suggests that the origin of the infrared emission in both radio-loud and radio-quiet sources is of thermal origin. Thus the source, or sources, of the infrared emission in NLS1 galaxies remains unclear. It is possible that non-thermal, reradiated (from torus), and star forming processes all contribute to the infrared emission. More infrared observations of large NLS1 samples are needed in order to study the origins of the infrared emission in more detail.

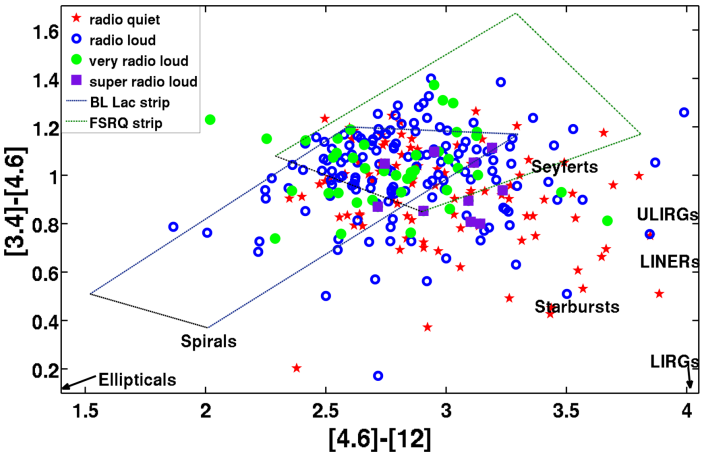

Fig. 8: WISE color-color diagram of our whole sample. γ-ray strips from Massaro et al. (2012) (BL Lac strip: dark blue dashed line, and FSRQ strip: dark green dashed line) and approximate regions populated by other types of sources are shown. Subsamples are shown with different symbols and colors; radio-quiet: filled red stars, radio-loud: open blue circles, very radio-loud: filled green circles, and super radio-loud: filled purple squares. See text for details.

Parent population. The results for the K-S test for luminosities, redshift, and black hole masses indicate that the parent population for the radio-loud and radio-quiet NLS1 sources is different. Still they have many similar properties, for example, the optical spectrum, which suggests that they are from the same or from very similar parent populations. To get an insight into the differences between the radio-loud and radio-quiet populations, a proper characterization of the host galaxies of radio-loud and radio-quiet sources is needed to see whether the differences might be related to the host galaxy type. Differences in black hole masses between the radio-quiet and radio-loud sources might also suggest an evolutionary line.

In our sample, radio-quiet sources tend to lie closer than radio-loud sources. This may also be related to AGN evolution; AGN were more numerous and luminous in the past. AGNs with more massive black holes – and thus higher luminosities – evolved first and were highly active in the past. They evolved to be less luminous or entirely quiescent sources, e.g., normal non-active galaxies. Low-luminosity sources with lower mass black holes emerged later and are much more numerous in the present Universe (Beckmann & Shrader 2012). Also the significant z – RL correlation (Pearson's r = 0.474, p=$\sim 10^{-18}$ and Spearman's $\rho = 0.497$, p=$\sim 10^{-19}$) supports these results; radio-quiet sources tend to lie closer than radio-loud.

In the current unification models differences between Type 1 and 2 Seyfert galaxies are explained with orientation and obscuration effects. In these models, Seyfert 1 galaxies are viewed pole-on, unobstructed, while Seyfert 2 galaxies are viewed edge-on through obscuring matter in the accretion disk (e.g. Miller & Antonucci (1983) and Antonucci (1993)). However, evidence against the simple unification model of Seyfert 1 and 2 galaxies has lately accumulated. Several studies have shown that approximately 50% of Seyfert 2 galaxies do not show a hidden broad-line region (HBLR) in their polarized optical spectra. This suggests that not all Seyfert 2 galaxies harbor a nucleus similar to Seyfert 1 galaxies. It seems that non-HBLR Seyfert 2 galaxies accommodate weaker nuclei that do not exhibit typical BLRs. HBLR and non-HBLR Seyfert 2 galaxies have also other differences such as luminosity and accretion rate (e.g., Tran (2001, 2003); Wu et al. (2011); Marinucci et al. (2012); Yu et al. (2013)). Zhang & Wang (2006) studied NLS1 and non-HBLR Seyfert 2 galaxies, and suggested that they can be unified based on orientation; non-HBLR Seyfert 2 galaxies are NLS1 galaxies viewed edge-on. This result is, however, debatable since the sources have many unexplained differences, for example, non-HBLR Seyfert 2 galaxies do not show Fe II emission lines (Yu et al. 2013). Furthermore, Decarli et al. (2008) studied the properties of NLS1 and BLS1 galaxies. They showed that when assuming a disk-like BLR and pole-on orientation of NLS1 galaxies, some of the observed differences between NLS1 and BLS1 galaxies can be explained.

AGN unification models are currently under constant revision; the question how NLS1 galaxies fit in remains open.

5. Summary

In this study the aim was to further our understanding about Narrow-Line Seyfert 1 galaxies, which are a new class of γ-ray emitting AGN. We addressed this issue by studying emission processes and properties of NLS1 galaxies, and also studied how these properties are connected with other AGN properties. To this end, we have compiled the largest multiwavelength database of NLS1 galaxies so far. This data set should be useful in the future as it permits easy identification and comparison of properties of new γ-ray NLS1 sources to be detected by Fermi or other facilities.

The main results of this study are:

1. The distributions of radio-quiet and radio-loud NLS1 galaxies in redshift, luminosity, and black hole mass are different. Radio-quiet sources also tend to lie closer than radio-loud sources.
2. NLS1 sources with more massive black holes are more likely to be able to lauch a powerful relativistic jet.
3. Multiwavelength correlations suggest that radio-loud sources host a jet which is the predominant sources of the radio, optical, and at least partially also X-ray emission. The origin of the infrared emission remains unclear.
4. Radio-quiet sources do not host a jet or the jet is very weak. Radio and infrared emission are more likely to originate from star formation processes, and optical and X-ray emission from the inner parts of the AGN.

While the results of this study mainly confirm what is already known of NLS1 galaxies, they also serve as a comprehensive starting point for further studies, for example, at high radio and infrared frequencies where the information so far is scarce. Open questions in need of more investigation include, for example, the origin of the infrared emission in NLS1 galaxies and the differences between radio-quiet and radio-loud sources (i.e. the question of the parent population). Simultaneous multiwavelength observations of especially radio-loud NLS1 sources should be very useful in modeling and understanding their emission properties. Studies of NLS1 galaxies may also provide us with a further look at AGN evolution and activity in general, and the evolution of relativistic jets.

Acknowledgements. We are grateful to K. I. I. Koljonen for his help with PCA. This research has made use of the NASA/IPAC Extragalactic Database (NED) which is operated by the Jet Propulsion Laboratory, California Institute of Technology, under contract with the National Aeronautics and Space Administration. The National Radio Astronomy Observatory is a facility of the National Science Foundation operated under cooperative agreement by Associated Universities, Inc. This publication makes use of data products from the Wide-field Infrared Survey Explorer, which is a joint project of the University of California, Los Angeles, and the Jet Propulsion Laboratory/California Institute of Technology, funded by the National Aeronautics and Space Administration. Funding for the Sloan Digital Sky Survey (SDSS) has been provided by the Alfred P. Sloan Foundation, the Participating Institutions, the National Aeronautics and Space Administration, the National Science Foundation, the U.S. Department of Energy, the Japanese Monbukagakusho, and the Max Planck Society. The SDSS Web site is http://www.sdss.org/. The SDSS is managed by the Astrophysical Research Consortium (ARC) for the Participating Institutions. The Participating Institutions are The University of Chicago, Fermilab, the Institute for Advanced Study, the Japan Participation Group, The Johns Hopkins University, the Korean Scientist Group, Los Alamos National Laboratory, the Max-Planck-Institute for Astronomy (MPIA), the Max-Planck-Institute for Astrophysics (MPA), New Mexico State University, University of Pittsburgh, University of Portsmouth, Princeton University, the United States Naval Observatory, and the University of Washington. This research has made use of the ROSAT All-Sky Survey data which have been processed at MPE.

References

Abdo, A. A., Ackermann, M., Ajello, M., et al. 2009a, ApJ, 699, 976
Abdo, A. A., Ackermann, M., Ajello, M., et al. 2009b, ApJ, 707, 727
Antonucci, R. 1993, ARA&A, 31, 473
Arshakian, T. G., Torrealba, J., Chavushyan, V. H., et al. 2010, A&A, 520, A62
Ballo, L., Heras, F. J. H., Barcons, X., & Carrera, F. J. 2012, A&A, 545, A66
Beckmann, V. & Shrader, C. R. 2012, Active Galactic Nuclei
Bentz, M. C., Peterson, B. M., Pogge, R. W., & Vestergaard, M. 2009, ApJ, 694, L166
Bianchi, S., Bonilla, N. F., Guainazzi, M., Matt, G., & Ponti, G. 2009, A&A, 501, 915
Boller, T., Brandt, W. N., & Fink, H. 1996, A&A, 305, 53
Boroson, T. A. 2002, ApJ, 565, 78
Boroson, T. A. & Green, R. F. 1992, ApJS, 80, 109
Botticella, M. T., Smartt, S. J., Kennicutt, R. C., et al. 2012, A&A, 537, A132
Bressan, A., Panuzzo, P., Buson, L., et al. 2006, ApJ, 639, L55
Brinkmann, W., Laurent-Muehleisen, S. A., Voges, W., et al. 2000, A&A, 356, 445
Castignani, G., Haardt, F., Lapi, A., et al. 2013, ArXiv e-prints
Chiaberge, M. & Marconi, A. 2011, MNRAS, 416, 917
Condon, J. J. 1992, ARA&A, 30, 575
Cutri, R. M. & et al. 2012, VizieR Online Data Catalog, 2311, 0
Decarli, R., Dotti, M., Fontana, M., & Haardt, F. 2008, MNRAS, 386, L15
Decarli, R., Dotti, M., & Treves, A. 2011, MNRAS, 413, 39
Doi, A., Nagira, H., Kawakatu, N., et al. 2012, ApJ, 760, 41
Dunlop, J. S., McLure, R. J., Kukula, M. J., et al. 2003, MNRAS, 340, 1095
Foschini, L. 2011, in Narrow-Line Seyfert 1 Galaxies and their Place in the Universe
Foschini, L., Ghisellini, G., Kovalev, Y. Y., et al. 2011, MNRAS, 413, 1671
Francis, P. J. & Wills, B. J. 1999, in Astronomical Society of the Pacific Conference Series, Vol. 162, Quasars and Cosmology, ed. G. Ferland & J. Baldwin, 363
Gliozzi, M., Papadakis, I. E., Grupe, D., et al. 2010, ApJ, 717, 1243
Goodrich, R. W. 1989, ApJ, 342, 224
Greene, J. E. & Ho, L. C. 2005, ApJ, 630, 122
Grupe, D. 2004, AJ, 127, 1799
Ho, L. C. 2002, ApJ, 564, 120
Jorstad, S. G., Marscher, A. P., Mattox, J. R., et al. 2001, ApJ, 556, 738
Kaspi, S., Smith, P. S., Netzer, H., et al. 2000, ApJ, 533, 631
Komossa, S. & Meerschweinchen, J. 2000, A&A, 354, 411
Komossa, S., Voges, W., Xu, D., et al. 2006, AJ, 132, 531

Lacy, M., Laurent-Muehleisen, S. A., Ridgway, S. E., Becker, R. H., & White, R. L. 2001, ApJ, 551, L17
Lähteenmäki, A. & Valtaoja, E. 2003, ApJ, 590, 95
Laor, A. 2000, ApJ, 543, L111
Laor, A. 2001, ApJ, 553, 677
Leighly, K. M. 1999, ApJS, 125, 297
León-Tavares, J., Valtaoja, E., Chavushyan, V. H., et al. 2011, MNRAS, 411, 1127
León-Tavares, J., Valtaoja, E., Giommi, P., et al. 2012, ApJ, 754, 23
Marinucci, A., Bianchi, S., Nicastro, F., Matt, G., & Goulding, A. D. 2012, ApJ, 748, 130
Mason, R. E., Ramos Almeida, C., Levenson, N. A., Nemmen, R., & Alonso-Herrero, A. 2013, ApJ, 777, 164
Massaro, F., D'Abrusco, R., Ajello, M., Grindlay, J. E., & Smith, H. A. 2011, ApJ, 740, L48
Massaro, F., D'Abrusco, R., Tosti, G., et al. 2012, ApJ, 750, 138
Mathur, S., Kuraszkiewicz, J., & Czerny, B. 2001, New A, 6, 321
McLure, R. J. & Jarvis, M. J. 2004, MNRAS, 353, L45
McLure, R. J., Kukula, M. J., Dunlop, J. S., et al. 1999, MNRAS, 308, 377
Metcalf, R. B. & Magliocchetti, M. 2006, MNRAS, 365, 101
Miller, J. S. & Antonucci, R. R. J. 1983, ApJ, 271, L7
Nieppola, E., Tornikoski, M., Valtaoja, E., et al. 2011, A&A, 535, A69
Ohta, K., Aoki, K., Kawaguchi, T., & Kiuchi, G. 2007, ApJS, 169, 1
Oshlack, A. Y. K. N., Webster, R. L., & Whiting, M. T. 2002, ApJ, 576, 81
Osterbrock, D. E. & Pogge, R. W. 1985, ApJ, 297, 166
Panessa, F., Barcons, X., Bassani, L., et al. 2007, A&A, 467, 519
Park, S., Sohn, B. W., & Yi, S. K. 2013, ArXiv e-prints
Peterson, B. M., McHardy, I. M., Wilkes, B. J., et al. 2000, ApJ, 542, 161
Puchnarewicz, E. M., Mason, K. O., Cordova, F. A., et al. 1992, MNRAS, 256, 589
Sani, E., Lutz, D., Risaliti, G., et al. 2010, MNRAS, 403, 1246
Snellen, I. A. G., Lehnert, M. D., Bremer, M. N., & Schilizzi, R. T. 2003, MNRAS, 342, 889
Tran, H. D. 2001, ApJ, 554, L19
Tran, H. D. 2003, ApJ, 583, 632
Urry, M. 2003, in Astronomical Society of the Pacific Conference Series, Vol. 290, Active Galactic Nuclei: From Central Engine to Host Galaxy, ed. S. Collin, F. Combes, & I. Shlosman, 3
Veron-Cetty, M. P. & Veron, P. 2003, VizieR Online Data Catalog, 7235, 0
Whalen, D. J., Laurent-Muehleisen, S. A., Moran, E. C., & Becker, R. H. 2006, AJ, 131, 1948
Woo, J.-H. & Urry, C. M. 2002a, ApJ, 579, 530
Woo, J.-H. & Urry, C. M. 2002b, ApJ, 581, L5
Woo, J.-H., Urry, C. M., van der Marel, R. P., Lira, P., & Maza, J. 2005, ApJ, 631, 762
Wright, E. L., Eisenhardt, P. R. M., Mainzer, A. K., et al. 2010, AJ, 140, 1868
Wu, Y.-Z., Zhang, E.-P., Liang, Y.-C., Zhang, C.-M., & Zhao, Y.-H. 2011, ApJ, 730, 121
Xu, D., Komossa, S., Zhou, H., et al. 2012, AJ, 143, 83
Younes, G., Porquet, D., Sabra, B., Reeves, J. N., & Grosso, N. 2012, A&A, 539, A104
Yu, P.-C., Huang, K.-Y., Hwang, C.-Y., & Ohyama, Y. 2013, ApJ, 768, 30
Yuan, W., Zhou, H. Y., Komossa, S., et al. 2008, ApJ, 685, 801
Zhang, E.-P. & Wang, J.-M. 2006, ApJ, 653, 137
Zhou, H., Wang, T., Yuan, W., et al. 2006, ApJS, 166, 128

Table 1: Flux densities of our whole sample.

Source	**FIRST** (mJy)	**W1** (mJy)	**W2** (mJy)	**W3** (mJy)	**W4** (mJy)	**SDSS** *u* (mJy)	**SDSS** *g* (mJy)	**SDSS** *r* (mJy)	**SDSS** *i* (mJy)	**SDSS** *z* (mJy)	**RASS** (mJy)
SDSS J002249.22-103956.2	1.88	1.73	2.94	7.22	16.44	0.26	0.35	0.37	0.41	0.53	
SDSS J002305.04-010743.4	10.56	0.60	0.60	2.29	3.15	0.16	0.24	0.35	0.46	0.52	
SDSS J002752.40+002615.7	4.59	1.92	2.68	7.61	17.61	0.12	0.16	0.22	0.33	0.33	
SDSS J013521.68-004402.1	1.99					0.23	0.52	0.83	1.23	1.49	0.0001
SDSS J014019.06-092110.5	2.12	1.81	1.91	10.29	12.81	0.34	0.76	1.26	1.81	2.20	0.00032
SDSS J014644.83-004043.2	4.33	4.06	3.94	19.07	42.52	0.49	1.06	1.67	2.47	2.65	
SDSS J022347.48-083655.6	1.04	1.53	2.08	3.83	11.16	0.11	0.13	0.18	0.17	0.25	0.0001
SDSS J022923.44-000047.9	2.43	0.74	1.11	2.26	7.23	0.09	0.12	0.12	0.15	0.15	
SDSS J023310.64-090940.9	2.18	1.19	1.69	3.06	8.00	0.14	0.18	0.21	0.21	0.30	
SDSS J024126.71-004526.3	2.58	0.74	1.30	3.13	6.39	0.17	0.21	0.22	0.23	0.24	
SDSS J024225.87-004142.6	29.03	0.09	0.13	0.43	1.31	0.02	0.02	0.03	0.03	0.05	
SDSS J024651.92-005931.0	2.08	2.39	3.78	8.76	17.31	0.54	0.69	0.70	0.80	0.84	
SDSS J025105.28-070230.2	5.80	1.13	1.76	7.75	36.36	0.07	0.13	0.24	0.24	0.44	
SDSS J025627.77-080135.0	16.38	0.92	1.45	4.57	9.34	0.29	0.32	0.31	0.32	0.31	
SDSS J030335.76+004145.0	1.51	0.35	0.49	1.15	2.27	0.04	0.08	0.10	0.13	0.14	
SDSS J030639.58+000343.2	3.65	5.35	6.39	16.10	40.44	0.53	0.91	1.42	2.17	2.47	0.00027
SDSS J073256.95+320136.5	1.39	0.83	1.67	4.59	8.67	0.02	0.03	0.03	0.04	0.05	
SDSS J073413.91+321722.8	0.83	0.27	0.29	0.75	3.30	0.07	0.09	0.13	0.15	0.21	
SDSS J073953.13+310220.9	6.66	1.32	2.25	5.82	9.35	0.11	0.15	0.22	0.22	0.32	
SDSS J074548.27+284838.0	1.15					0.19	0.35	0.53	0.74	0.84	0.0001
SDSS J074631.78+354523.7	2.62	1.43	2.36	6.93	14.32	0.07	0.15	0.17	0.22	0.22	
SDSS J074636.53+430206.7	2.20	0.77	1.05	2.16	5.78	0.10	0.12	0.12	0.14	0.14	
SDSS J075101.42+291419.2	1.52	5.40	7.29	18.72	45.48	0.68	0.93	1.10	1.61	1.57	
SDSS J075141.57+353914.8	1.26	0.43	0.54	2.42	6.57	0.05	0.07	0.11	0.14	0.19	
SDSS J075209.09+414235.5	2.70	0.41	0.63	1.40	5.06	0.16	0.17	0.21	0.23	0.26	0.00012
SDSS J075838.14+414512.5	2.14	3.38	4.03	16.41	77.95	0.16	0.54	0.97	1.45	1.82	0.00006
SDSS J080037.63+461257.9	1.44	1.50	1.91	7.08	18.66	0.14	0.25	0.44	0.60	0.67	
SDSS J080203.03+435940.3	4.13	0.93	0.61	1.36	3.18	0.15	0.35	0.70	1.11	1.51	
SDSS J080306.76+302411.9	0.83	0.35	0.43	1.56	2.35	0.05	0.07	0.10	0.11	0.14	
SDSS J080409.24+385348.8	2.68	6.12	8.56	18.60	59.04	0.17	0.32	0.57	0.88	0.84	
SDSS J080514.10+285607.2	0.75	0.35	0.29	1.29	4.26	0.05	0.08	0.16	0.24	0.27	
SDSS J080535.17+302201.7	60.81	0.81	1.15	2.98	8.07	0.09	0.11	0.11	0.13	0.13	
SDSS J080710.87+245106.0	4.40	0.41	0.52	1.21	4.25	0.09	0.10	0.12	0.12	0.20	0.00006
SDSS J081206.67+394017.2	1.80	0.34	0.52	1.63	5.98	0.02	0.03	0.05	0.06	0.08	
SDSS J081432.11+560956.6	80.24	0.64	0.96	1.96	3.33	0.21	0.25	0.22	0.25	0.23	0.00017
SDSS J081516.87+460430.9	5.86	10.80	11.04	58.55	187.50	1.46	3.85	6.63	9.36	12.25	0.00044
SDSS J081849.27+383416.1	2.08	1.60	1.84	6.10	13.51	0.30	0.37	0.51	0.67	0.79	
SDSS J082007.81+372839.7	1.64	3.32	2.73	11.88	22.13	0.50	1.58	3.22	4.89	6.61	0.00012
SDSS J082244.88+460318.1	21.63	0.39	0.62	1.05	1.96	0.12	0.13	0.13	0.12	0.20	
SDSS J082319.23+482516.5	0.89	0.97	1.24	2.95	6.26	0.10	0.14	0.21	0.30	0.35	
SDSS J082405.19+445246.1	1.16	1.37	1.83	10.16	16.15	0.21	0.25	0.33	0.43	0.48	
SDSS J082433.33+380013.1	2.07	1.98	1.79	8.83	14.93	0.50	0.88	1.31	1.83	2.11	

Continued on next page

Table 1 – *Continued from previous page*

Source	FIRST (mJy)	W1 (mJy)	W2 (mJy)	W3 (mJy)	W4 (mJy)	SDSS *u* (mJy)	SDSS *g* (mJy)	SDSS *r* (mJy)	SDSS *i* (mJy)	SDSS *z* (mJy)	RASS (mJy)
SDSS J082700.24+374822.1	150.31	0.18	0.22	0.49	2.83	0.03	0.03	0.04	0.04	0.04	
SDSS J083037.75+042127.8	2.22	0.73	1.15	2.54	6.91	0.11	0.15	0.14	0.16	0.15	
SDSS J083130.01+392203.6	1.52	0.56	0.61	1.32	3.13	0.08	0.10	0.18	0.25	0.30	
SDSS J083317.45+512422.4	0.70	0.88	1.28	2.68	7.62	0.09	0.18	0.23	0.31	0.31	0.00011
SDSS J083943.59+433018.0	2.15	0.73	0.96	2.41	6.86	0.08	0.13	0.22	0.35	0.38	
SDSS J084310.79+395345.1	2.17	0.75	1.13	3.06	10.19	0.17	0.23	0.26	0.28	0.32	
SDSS J084610.14+445150.9	6.10	0.54	0.81	1.61	2.94	0.05	0.08	0.08	0.10	0.10	
SDSS J084744.55+442610.7	5.99	0.51	0.67	1.08	3.83	0.04	0.06	0.08	0.11	0.13	
SDSS J084837.66+053237.8	0.77	0.43	0.63	1.23	2.52	0.06	0.08	0.08	0.10	0.10	
SDSS J084940.72+374618.3	1.40	0.79	0.84	2.25	3.82	0.13	0.16	0.24	0.35	0.39	
SDSS J084957.98+510829.0	350.53	0.76	0.96	3.05	7.26	0.04	0.11	0.19	0.32	0.46	
SDSS J085001.17+462600.5	21.29	0.45	0.50	0.75	1.90	0.04	0.08	0.11	0.15	0.15	
SDSS J085152.63+522833.0	3.74					0.36	0.96	1.56	2.16	2.65	0.0003
SDSS J085338.27+033246.1	4.04	1.43	1.75	6.43	11.57	0.10	0.24	0.44	0.63	0.73	
SDSS J085457.22+544820.6	1.31	1.09	1.38	5.88	19.31	0.13	0.15	0.22	0.36	0.47	0.00011
SDSS J085555.53+434416.8	6.27	0.89	1.26	2.38	8.07	0.06	0.10	0.11	0.15	0.16	
SDSS J085613.17+363144.8	2.53	0.41	0.43	0.83	2.36	0.06	0.10	0.18	0.27	0.34	
SDSS J085907.58+044434.4	1.70	0.42	0.61	1.75	5.21	0.11	0.11	0.13	0.17	0.17	
SDSS J090015.28+510800.2	17.09	3.19	4.51	14.17	38.32	0.31	0.37	0.50	0.80	0.76	0.00031
SDSS J090113.23+465734.7	1.55	0.43	0.51	1.61	3.24	0.06	0.08	0.10	0.12	0.14	
SDSS J090157.12+063734.6	7.62	0.20	0.35	0.41	3.54	0.03	0.04	0.04	0.05	0.05	
SDSS J090227.16+044309.6	156.47	0.83	0.97	3.12	10.47	0.06	0.10	0.13	0.19	0.23	
SDSS J090335.47+013224.3	2.25	1.28	2.28	7.45	16.47	0.22	0.25	0.28	0.28	0.35	
SDSS J090359.91+363054.7	2.05	1.59	2.57	8.42	25.95	0.00	0.02	0.07	0.10	0.20	
SDSS J090448.20+420220.0	2.79	0.71	0.99	1.95	4.87	0.12	0.14	0.16	0.20	0.20	0.00013
SDSS J091146.07+403501.1	3.03	0.64	1.08	3.07	6.36	0.05	0.08	0.14	0.18	0.21	
SDSS J091313.73+365817.2	7.72	3.24	4.34	16.65	40.72	0.31	0.48	0.67	0.99	1.10	0.00022
SDSS J091513.90+571233.2	1.75	0.19	0.17	0.78	2.32	0.02	0.04	0.07	0.10	0.12	
SDSS J092216.63+384448.0	4.54					0.06	0.09	0.09	0.10	0.08	
SDSS J092613.80+065056.5	3.83	3.18	3.52	22.51	64.36	0.39	0.72	0.95	1.50	1.57	0.00012
SDSS J092704.38+563351.6	8.46	0.34	0.47	1.67	4.30	0.07	0.09	0.13	0.17	0.18	
SDSS J092715.93+020330.7	1.03	1.09	2.16	7.78	17.69	0.04	0.09	0.16	0.20	0.32	
SDSS J092856.27+013246.0	0.70	1.19	1.72	4.52	9.80	0.09	0.11	0.16	0.17	0.24	0.00014
SDSS J093027.87+514141.3	2.37	0.65	1.04	2.30	4.51	0.12	0.17	0.17	0.20	0.18	
SDSS J093034.79+570520.8	1.27	0.56	0.86	1.62	3.96	0.10	0.12	0.12	0.13	0.13	
SDSS J093048.27+404447.3	0.98	0.92	1.10	2.20	3.98	0.12	0.15	0.19	0.28	0.29	0.00029
SDSS J093609.14-002639.8	0.70	1.91	2.56	7.18	17.29	0.20	0.26	0.39	0.57	0.62	0.00009
SDSS J094028.33+043146.1	0.84	0.45	0.62	1.29	3.88	0.07	0.08	0.10	0.11	0.17	0.00005
SDSS J094121.34+011147.8	1.91	0.97	1.52	3.66	9.04	0.12	0.16	0.20	0.23	0.26	
SDSS J094422.14+103739.8	1.67	1.05	1.34	2.15	2.52	0.19	0.21	0.26	0.30	0.31	
SDSS J094554.40+423840.0	1.50	6.27	6.55	18.58	49.55	0.74	1.51	2.42	3.58	4.32	0.00019
SDSS J094621.27+471131.3	1.71	1.11	1.62	3.68	7.68	0.25	0.24	0.27	0.38	0.36	0.00018
SDSS J094704.52+472143.0	2.84	2.27	3.74	9.73	29.36	0.12	0.22	0.28	0.34	0.33	0.00023

Continued on next page

Table 1 – *Continued from previous page*

Source	FIRST (mJy)	W1 (mJy)	W2 (mJy)	W3 (mJy)	W4 (mJy)	SDSS *u* (mJy)	SDSS *g* (mJy)	SDSS *r* (mJy)	SDSS *i* (mJy)	SDSS *z* (mJy)	RASS (mJy)
SDSS J094842.67+502931.5	5.83	15.41	20.02	64.14	189.06	0.94	2.16	3.13	4.47	5.48	0.00005
SDSS J094857.32+002225.5	111.46	1.60	2.44	6.93	14.61	0.13	0.16	0.17	0.21	0.21	0.00013
SDSS J095257.15+050910.3	6.01	2.50	3.93	6.69	9.24	0.43	0.55	0.56	0.62	0.56	
SDSS J095317.09+283601.5	47.94	0.37	0.48	0.93	2.51	0.07	0.09	0.09	0.11	0.12	
SDSS J095449.94+070444.7	3.04	0.44	0.64	1.04	3.50	0.14	0.19	0.19	0.22	0.20	
SDSS J095650.14+515212.2	1.31	2.05	3.58	8.50	16.59	0.24	0.36	0.40	0.48	0.49	
SDSS J095823.74+011235.8	1.65	0.38	0.66	2.70	7.58	0.03	0.05	0.07	0.10	0.12	
SDSS J095833.95+560224.5	0.83	0.61	0.80	2.57	6.17	0.13	0.16	0.20	0.24	0.24	0.00016
SDSS J095941.37+491529.5	7.28	14.44	21.10	63.78	125.03	0.20	0.79	1.70	2.88	3.97	0.00005
SDSS J100253.51+513709.4	1.04	0.95	1.32	8.07	13.65	0.08	0.14	0.25	0.35	0.47	
SDSS J100405.00-003253.4	2.55	1.94	2.84	9.33	21.31	0.09	0.14	0.21	0.24	0.35	
SDSS J100633.91+430923.4	12.29	0.43	0.67	1.43	4.20	0.07	0.12	0.11	0.12	0.11	
SDSS J101435.46+433056.5	20.03	0.40	0.64	1.24	2.67	0.05	0.07	0.08	0.10	0.10	
SDSS J101549.33+424243.0	2.22	0.43	0.55	1.04	2.38	0.08	0.10	0.09	0.10	0.11	
SDSS J101645.11+421025.5	1.47	9.67	13.26	34.16	72.68	1.14	1.60	2.11	3.01	3.38	0.00076
SDSS J101734.76+473149.0	2.75	0.56	0.94	3.06	7.42	0.10	0.13	0.13	0.14	0.17	0.00003
SDSS J101813.99+054625.5	4.99	1.83	2.98	6.93	17.19	0.20	0.28	0.27	0.32	0.38	
SDSS J101936.27+002029.7	10.39	0.92	1.22	1.78	3.64	0.10	0.15	0.23	0.34	0.38	
SDSS J102000.45+623944.7	1.36	1.40	1.63	5.22	9.63	0.12	0.24	0.43	0.65	0.81	0.00007
SDSS J102049.47+534539.2	0.70	0.63	0.80	3.94	11.86	0.06	0.08	0.09	0.11	0.12	
SDSS J102148.90+030732.2	1.24	2.22	1.94	7.22	19.89	0.26	0.85	1.55	2.24	2.83	
SDSS J102256.62+540718.0	0.87	0.78	1.18	3.62	7.91	0.07	0.09	0.13	0.11	0.20	0.00004
SDSS J102402.60+062943.9	2.26	2.77	2.72	8.39	15.57	0.57	1.31	2.09	2.77	3.37	0.00028
SDSS J102531.28+514034.9	0.60	11.21	12.91	26.54	49.34	1.27	1.70	2.29	3.05	3.69	0.00304
SDSS J103123.73+423439.3	16.95	0.64	0.92	1.96	3.46	0.06	0.08	0.13	0.16	0.25	
SDSS J103128.98+091607.2	9.89	0.40	0.57	1.45	3.54	0.05	0.08	0.07	0.09	0.08	
SDSS J103210.16+065205.4	1.41	4.28	5.03	12.89	35.15	0.13	0.64	1.22	1.75	2.31	
SDSS J103352.23+521139.3	0.95	0.65	1.22	3.34	8.39	0.11	0.08	0.14	0.17	0.17	
SDSS J103430.53+470820.1	53.82	0.99	1.62	5.33	12.83	0.19	0.23	0.23	0.23	0.23	
SDSS J103457.29-010209.1	4.79	0.94	1.32	3.14	4.85	0.27	0.32	0.35	0.34	0.47	0.00012
SDSS J103615.68+031916.7	1.06	0.73	1.02	2.63	8.06	0.15	0.17	0.17	0.18	0.24	
SDSS J103727.45+003635.6	27.94	0.29	0.53	1.53	2.50	0.03	0.06	0.08	0.10	0.11	
SDSS J104541.76+520235.5	1.17	4.69	7.22	18.93	44.08	0.59	0.68	0.76	0.70	1.06	0.00039
SDSS J104732.68+472532.1	767.43	0.38	0.59	2.06	5.56	0.07	0.09	0.11	0.13	0.16	0.00004
SDSS J104808.25+551954.7	0.60	0.38	0.50	0.95	1.57	0.05	0.07	0.08	0.10	0.12	
SDSS J105547.44+492950.8	1.48	0.70	0.96	1.44	2.63	0.04	0.06	0.08	0.12	0.14	
SDSS J105558.16+552310.4	1.22	1.33	1.99	5.26	8.79	0.03	0.06	0.08	0.11	0.12	
SDSS J110333.01+083449.0	1.71	1.60	2.19	6.06	17.87	0.09	0.17	0.27	0.38	0.44	0.00005
SDSS J110423.64+503404.3	1.11	1.95	2.33	4.90	11.29	0.10	0.20	0.36	0.58	0.69	0.00007
SDSS J110542.72+020250.9	212.83	0.42	0.48	1.61	4.40	0.10	0.11	0.12	0.14	0.15	0.00018
SDSS J110703.76+004202.3	2.75	0.75	1.22	2.42	3.91	0.14	0.18	0.17	0.20	0.18	
SDSS J110747.83+013933.5	1.45	0.21	0.34	0.62	2.13	0.06	0.08	0.08	0.09	0.09	
SDSS J110931.25+632623.4	1.52	0.48	0.61	1.36	2.08	0.06	0.08	0.10	0.13	0.15	0.00003

Continued on next page

Table 1 – *Continued from previous page*

Source	FIRST (mJy)	W1 (mJy)	W2 (mJy)	W3 (mJy)	W4 (mJy)	SDSS *u* (mJy)	SDSS *g* (mJy)	SDSS *r* (mJy)	SDSS *i* (mJy)	SDSS *z* (mJy)	RASS (mJy)
SDSS J111005.03+365336.3	20.83	0.12	0.15	0.40	2.01	0.01	0.02	0.02	0.04	0.04	
SDSS J111340.41+040211.2	1.70	0.33	0.45	1.45	3.79	0.07	0.09	0.12	0.14	0.18	
SDSS J111450.07+502917.2	6.49	0.27	0.35	0.83	2.90	0.06	0.08	0.08	0.10	0.11	
SDSS J111756.86-000220.6	15.12	0.36	0.58	0.86	2.16	0.06	0.08	0.08	0.09	0.10	
SDSS J111934.01+533518.7	17.25	10.04	14.64	54.89	127.00	0.23	0.77	1.55	2.66	3.46	
SDSS J112016.17+491428.8	12.24	0.40	0.60	1.77	2.41	0.05	0.07	0.13	0.19	0.21	
SDSS J112042.75+084131.2	0.85	1.53	2.15	6.24	13.57	0.08	0.13	0.23	0.25	0.36	
SDSS J112108.59+535121.1	2.60	15.37	20.71	37.28	85.19	0.65	1.01	1.41	2.48	2.24	0.00046
SDSS J112114.22+032546.8	2.20	5.61	7.93	17.96	49.20	0.45	0.49	0.58	0.85	0.85	0.00021
SDSS J112444.54+040927.1	1.90	0.85	1.14	2.72	6.71	0.07	0.10	0.16	0.22	0.27	
SDSS J112521.60+052358.2	33.20	0.75	1.04	2.61	4.35	0.06	0.07	0.10	0.12	0.15	
SDSS J112702.72+030152.0	9.22	0.64	0.92	2.82	7.18	0.06	0.08	0.10	0.12	0.16	
SDSS J112813.03+102308.3	1.13	12.53	17.12	37.80	79.72	0.85	1.27	1.68	2.29	2.53	
SDSS J112941.94+512050.7	1.26	1.25	1.75	6.76	14.95	0.36	0.46	0.57	0.71	0.69	0.00045
SDSS J113001.89+494434.8	0.79	1.37	1.88	4.14	8.68	0.21	0.28	0.38	0.46	0.50	0.00014
SDSS J113055.88+024800.0	3.17	0.46	0.62	1.69	5.65	0.05	0.06	0.10	0.11	0.16	
SDSS J113320.91+043255.2	5.02	1.02	1.41	2.73	7.97	0.17	0.19	0.24	0.30	0.33	
SDSS J113427.09+100113.0	1.35	1.13	1.72	4.79	13.13	0.03	0.09	0.16	0.26	0.31	
SDSS J113452.07+563723.9	1.34	0.46	0.59	1.42	4.27	0.05	0.06	0.11	0.12	0.15	
SDSS J113625.42+100523.2	1.45	2.35	3.67	8.42	18.42	0.21	0.30	0.31	0.39	0.40	0.00009
SDSS J113824.54+365327.1	12.62	0.76	0.99	1.84	4.70	0.02	0.05	0.11	0.14	0.22	
SDSS J114256.64+042731.4	0.69	0.88	1.28	5.88	23.41	0.13	0.20	0.24	0.27	0.31	
SDSS J114654.28+323652.3	15.42	0.74	0.93	1.93	3.24	0.08	0.13	0.16	0.18	0.20	0.00003
SDSS J114805.31-023303.6	4.24	1.32	2.13	4.48	8.77	0.22	0.31	0.31	0.34	0.33	
SDSS J114954.99+044812.9	1.76	3.16	4.89	12.48	28.31	0.38	0.42	0.51	0.48	0.64	0.00015
SDSS J115215.84+042456.2	3.11	0.83	0.78	1.74	4.91	0.10	0.23	0.45	0.69	0.84	
SDSS J115507.61+520129.6	2.05	2.42	2.87	13.75	34.44	0.48	0.60	0.78	1.01	1.11	0.00008
SDSS J115544.40+040631.6	0.77	2.03	2.24	9.23	24.22	0.21	0.33	0.52	0.74	0.87	0.00007
SDSS J115636.54+020827.1	2.07	1.02	1.59	3.21	7.43	0.04	0.08	0.11	0.14	0.16	
SDSS J115637.77+051633.6	2.13	0.23	0.25	0.36	3.45	0.05	0.06	0.08	0.10	0.12	
SDSS J115644.79+110228.1	1.44	0.34	0.38	0.44	3.61	0.05	0.06	0.06	0.08	0.09	
SDSS J115753.20-031537.1	2.58	5.47	7.80	22.03	68.64	0.25	0.29	0.48	0.77	0.71	
SDSS J120014.08-004638.7	21.84	1.68	2.04	3.48	6.75	0.11	0.14	0.27	0.47	0.50	0.00036
SDSS J120113.77-024241.3	0.80	1.93	2.63	5.80	14.28	0.02	0.04	0.11	0.15	0.26	
SDSS J120226.76-012915.3	12.40	10.26	15.67	53.64	196.34	0.47	0.60	0.85	1.18	1.39	0.00033
SDSS J120628.98+503001.5	1.15	0.94	1.24	4.20	14.54	0.09	0.13	0.22	0.33	0.35	
SDSS J120652.44+515918.7	1.32	0.48	0.71	4.61	20.48	0.08	0.09	0.10	0.10	0.13	0.00005
SDSS J120700.30-021927.2	2.01	2.23	3.32	6.06	14.60	0.08	0.13	0.20	0.21	0.33	
SDSS J120806.90-013509.7	2.65	0.38	0.64	1.59	3.49	0.08	0.12	0.10	0.11	0.13	
SDSS J121325.48+092319.5	1.54	1.50	2.24	5.66	16.08	0.07	0.12	0.16	0.18	0.22	
SDSS J121549.44+544224.0	2.35	6.84	9.95	32.00	75.55	0.58	0.75	0.93	1.26	1.27	0.00018
SDSS J121845.55-012545.8	5.31	0.48	0.64	1.39	2.23	0.10	0.11	0.14	0.17	0.17	
SDSS J122102.95-000733.8	0.60	0.83	1.35	7.22	14.51	0.05	0.10	0.17	0.20	0.29	0.00009

Continued on next page

Table 1 – *Continued from previous page*

Source	FIRST (mJy)	W1 (mJy)	W2 (mJy)	W3 (mJy)	W4 (mJy)	SDSS *u* (mJy)	SDSS *g* (mJy)	SDSS *r* (mJy)	SDSS *i* (mJy)	SDSS *z* (mJy)	RASS (mJy)
SDSS J122753.10+024215.8	5.06	1.52	2.16	3.64	7.03	0.12	0.13	0.16	0.16	0.27	
SDSS J123417.88+102543.0	2.53	2.34	4.05	11.01	21.61	0.12	0.17	0.25	0.23	0.44	
SDSS J123852.12+394227.8	11.22	0.24	0.30	0.66	2.75	0.04	0.05	0.06	0.08	0.07	0.0001
SDSS J124634.65+023809.0	38.06	0.71	1.01	2.33	7.30	0.13	0.16	0.18	0.19	0.24	
SDSS J124635.25+022208.8	2.23	6.89	10.18	40.80	103.04	1.04	1.42	1.70	2.10	2.31	0.00305
SDSS J125051.05+060910.0	2.52	2.44	3.15	11.40	29.88	0.30	0.41	0.58	0.80	0.84	
SDSS J125337.36-004809.6	0.67	0.87	1.42	3.23	7.18	0.13	0.15	0.15	0.15	0.18	0.00006
SDSS J125635.89+500852.4	209.08	0.49	0.71	1.64	4.50	0.05	0.01	0.10	0.12	0.13	0.00006
SDSS J130034.40+501112.8	1.51	0.45	0.66	1.23	2.69	0.07	0.09	0.09	0.10	0.10	
SDSS J130052.11+564105.9	23.94	3.76	5.41	14.12	28.99	0.39	0.55	0.72	1.06	1.09	0.00013
SDSS J130522.75+511640.3	86.94	1.55	2.84	8.53	17.55	0.36	0.44	0.51	0.53	0.57	
SDSS J130916.67-001550.2	0.89	0.75	1.21	2.51	3.97	0.06	0.08	0.09	0.10	0.11	
SDSS J131136.36+580801.6	3.10	1.15	0.77	1.27	3.72	0.12	0.42	0.88	1.35	1.67	0.00004
SDSS J132206.76+561213.0	1.46	1.01	1.59	3.40	8.14	0.02	0.06	0.11	0.17	0.17	
SDSS J132447.10+530257.7	29.16	0.34	0.38	0.96	3.01	0.03	0.05	0.09	0.12	0.16	
SDSS J132832.51-010318.0	1.75	0.38	0.62	1.40	3.17	0.06	0.08	0.08	0.09	0.12	
SDSS J133138.04+013151.7	2.99	2.49	2.61	6.39	20.74	0.17	0.41	0.80	1.26	1.50	0.00018
SDSS J133450.44+010218.8	1.70	1.18	1.51	4.20	7.00	0.09	0.13	0.23	0.33	0.41	
SDSS J133619.63+540150.9	2.71	0.48	0.78	1.38	3.85	0.09	0.12	0.11	0.12	0.13	
SDSS J133724.33+600541.7	4.56	0.66	0.90	2.59	8.33	0.12	0.14	0.17	0.21	0.21	
SDSS J133757.03+565631.3	0.74	0.74	1.02	1.91	3.69	0.08	0.11	0.13	0.13	0.19	0.00004
SDSS J133819.96-025250.8	8.31	0.86	1.32	3.16	8.09	0.08	0.12	0.14	0.17	0.16	
SDSS J134206.57+050523.9	3.85	5.93	9.47	31.76	68.96	0.47	0.51	0.64	0.66	0.87	0.00015
SDSS J134426.42+441620.1	11.59	5.31	5.74	15.39	25.55	1.20	2.29	3.10	4.33	5.07	0.00022
SDSS J135121.43+481355.8	1.58	0.27	0.47	1.06	2.24	0.06	0.01	0.09	0.09	0.09	
SDSS J135516.55+561244.7	6.29	4.29	4.88	15.09	48.64	0.59	0.69	0.87	1.31	1.22	0.00095
SDSS J135618.50-011514.0	4.32	0.48	0.64	1.30	2.97	0.06	0.01	0.10	0.12	0.13	
SDSS J135908.01+002731.9	2.46	0.88	1.28	2.90	6.98	0.08	0.12	0.19	0.24	0.30	
SDSS J140130.81+570453.2	1.03	0.69	1.00	2.41	7.57	0.10	0.13	0.14	0.16	0.20	0.00005
SDSS J140322.11+022232.9	3.96	0.51	0.59	2.01	5.50	0.03	0.05	0.12	0.17	0.24	
SDSS J140914.36+565625.7	2.81	2.42	3.31	6.23	15.72	0.04	0.12	0.25	0.37	0.44	0.00007
SDSS J141049.55+015135.0	2.09	0.90	1.00	6.38	20.69	0.08	0.15	0.25	0.38	0.44	0.00007
SDSS J141700.54+415219.2	1.21	0.55	0.85	2.36	5.25	0.13	0.15	0.14	0.16	0.14	
SDSS J142033.71+573901.0	3.83	1.31	2.57	7.18	16.26	0.01	0.05	0.13	0.21	0.36	
SDSS J142441.21-000727.2	3.10	0.77	1.01	2.09	5.79	0.12	0.17	0.20	0.20	0.32	0.00027
SDSS J142830.17+555931.3	6.44	0.60	0.77	1.12	1.68	0.08	0.08	0.10	0.11	0.15	
SDSS J143249.69+451338.3	3.05	0.87	1.15	2.73	7.05	0.12	0.13	0.14	0.13	0.23	0.00005
SDSS J143453.83+592626.4	1.28	0.67	1.13	2.27	3.36	0.14	0.18	0.18	0.19	0.22	
SDSS J143509.49+313147.8	44.72	0.54	0.71	3.23	7.25	0.04	0.06	0.08	0.10	0.09	0.00018
SDSS J143701.20-010418.1	1.89	1.27	1.67	4.87	11.44	0.07	0.09	0.15	0.20	0.31	
SDSS J143952.92+392359.0	1.11	2.42	4.07	15.61	42.13	0.12	0.19	0.27	0.45	0.44	
SDSS J144012.76+615633.2	2.88	5.19	7.27	14.43	49.61	0.48	0.56	0.67	0.60	0.88	0.00037
SDSS J144043.34+613008.8	1.21	0.32	0.37	0.86	3.89	0.09	0.10	0.11	0.13	0.13	

Continued on next page

Table 1 – *Continued from previous page*

Source	FIRST (mJy)	W1 (mJy)	W2 (mJy)	W3 (mJy)	W4 (mJy)	SDSS *u* (mJy)	SDSS *g* (mJy)	SDSS *r* (mJy)	SDSS *i* (mJy)	SDSS *z* (mJy)	RASS (mJy)
SDSS J144303.81+035749.8	0.86	0.44	0.51	1.06	2.04	0.04	0.07	0.11	0.18	0.19	
SDSS J144318.56+472556.7	171.12	1.37	2.08	5.81	15.35	0.18	0.20	0.20	0.21	0.23	0.00004
SDSS J144751.79+505328.8	1.40	1.05	1.64	4.78	10.50	0.10	0.12	0.16	0.16	0.25	0.00003
SDSS J144848.67+372935.7	37.87	0.43	0.52	1.55	4.88	0.05	0.07	0.10	0.13	0.15	
SDSS J144855.21+575503.5	1.41	0.34	0.46	0.73	2.39	0.08	0.10	0.10	0.12	0.11	0.00015
SDSS J144903.19+503018.2	0.69	0.66	1.21	3.25	7.52	0.05	0.08	0.09	0.11	0.10	
SDSS J145041.93+591936.9	3.44					0.12	0.16	0.27	0.39	0.41	
SDSS J145751.91+000011.5	2.95	0.19	0.20	0.28	2.14	0.04	0.07	0.13	0.17	0.19	
SDSS J150225.27+490220.7	1.91	0.94	0.84	5.52	16.33	0.28	0.59	0.92	1.27	1.47	0.00006
SDSS J150506.48+032630.8	380.49	0.75	0.99	3.58	10.73	0.11	0.14	0.20	0.25	0.33	
SDSS J150521.92+014149.8	1.52	1.12	1.28	2.73	5.44	0.21	0.27	0.33	0.41	0.42	0.00005
SDSS J150734.51+403627.9	1.18	0.56	0.62	1.55	3.12	0.11	0.15	0.27	0.34	0.43	0.00008
SDSS J150832.91+583422.5	4.35	0.20	0.29	0.56	1.65	0.02	0.03	0.04	0.05	0.05	
SDSS J151131.33+502219.0	2.44	1.19	1.98	9.42	20.30	0.13	0.18	0.27	0.38	0.42	
SDSS J151617.16+472805.1	25.15	0.70	0.78	1.52	2.99	0.10	0.15	0.29	0.45	0.56	0.00008
SBS1517+520	5.97	1.54	2.55	6.01	16.43	0.17	0.23	0.27	0.28	0.47	0.00003
SDSS J152205.41+393441.3	2.52					0.34	1.38	3.21	4.87	6.98	
SDSS J152429.34+351522.1	3.97	1.08	1.47	6.34	13.52	0.08	0.13	0.21	0.28	0.34	
SDSS J152628.19-003809.5	1.64	1.81	2.35	11.17	26.00	0.26	0.37	0.50	0.72	0.77	0.0001
SDSS J152829.40+033027.7	2.45	0.62	0.96	3.34	11.08	0.09	0.10	0.12	0.12	0.19	
SDSS J153243.67-004342.5	5.85	0.55	0.86	3.19	8.67	0.09	0.09	0.11	0.11	0.19	
SDSS J153705.95+005522.8	1.01	3.14	3.74	14.91	23.58	0.42	0.63	0.90	1.27	1.40	0.00008
SDSS J153732.62+494247.7	1.43	0.35	0.56	2.10	4.68	0.12	0.13	0.16	0.15	0.20	0.00078
SDSS J153903.95+571605.9	1.38					0.05	0.06	0.07	0.08	0.08	
SDSS J153911.16+002600.7	0.93	1.28	1.71	6.40	15.51	0.15	0.17	0.24	0.26	0.37	0.00009
SDSS J154530.24+484609.1	2.11	8.04	12.55	38.29	97.32	0.87	0.97	0.97	0.96	1.22	0.00022
SDSS J154653.02+571013.7	1.10	1.87	2.99	6.09	10.87	0.13	0.15	0.18	0.20	0.22	
SDSS J154817.92+351128.0	141.51	0.96	1.33	3.40	10.59	0.18	0.23	0.23	0.25	0.25	0.00013
SDSS J154830.89+563012.1	2.07	0.36	0.40	1.36	1.75	0.08	0.11	0.11	0.13	0.14	
SDSS J155433.22+453646.4	1.32	0.86	1.52	11.07	18.65	0.04	0.07	0.10	0.14	0.15	
SDSS J155451.14+461917.4	0.91	2.03	2.43	7.33	14.22	0.09	0.23	0.44	0.73	0.92	
SDSS J155609.81+030922.3	1.05	6.87	8.76	26.44	47.49	0.43	0.60	0.91	1.46	1.63	0.00013
SDSS J155936.14+544203.9	4.20	0.99	1.52	4.99	13.89	0.14	0.16	0.19	0.18	0.27	
SDSS J160404.53+493820.5	2.32	0.32	0.36	0.37	1.98	0.04	0.05	0.07	0.11	0.11	
SDSS J160424.17+271759.1	1.13	0.79	1.44	3.49	8.08	0.08	0.11	0.14	0.15	0.16	
SDSS J160452.44+473320.1	0.97	0.37	0.59	1.46	3.92	0.10	0.13	0.14	0.13	0.14	
SDSS J160518.50+375653.4	121.80	3.47	5.22	13.60	30.55	0.43	0.48	0.54	0.68	0.62	0.00024
SDSS J160558.12+440319.5	2.34					0.49	1.78	3.47	4.99	6.49	
SDSS J161301.87+524749.6	1.35	0.34	0.42	1.55	2.92	0.10	0.11	0.12	0.14	0.14	
SDSS J162012.76+400906.2	0.89	4.34	3.40	9.25	11.54	1.20	2.67	4.35	5.51	6.94	0.00062
SDSS J162348.97+392503.5	6.84	0.38	0.58	1.39	4.35	0.07	0.09	0.10	0.11	0.11	
SDSS J162458.42+423107.5	2.09	0.39	0.58	1.68	4.59	0.05	0.09	0.13	0.18	0.20	0.00013
SDSS J162543.14+490059.0	6.80	0.35	0.53	1.02	2.36	0.04	0.06	0.06	0.08	0.08	

Continued on next page

Table 1 – *Continued from previous page*

Source	**FIRST** (mJy)	**W1** (mJy)	**W2** (mJy)	**W3** (mJy)	**W4** (mJy)	**SDSS** *u* (mJy)	**SDSS** *g* (mJy)	**SDSS** *r* (mJy)	**SDSS** *i* (mJy)	**SDSS** *z* (mJy)	**RASS** (mJy)
SDSS J162611.87+372536.2	0.95	0.67	1.10	2.26	3.56	0.12	0.16	0.16	0.19	0.16	0.00004
SDSS J162750.56+473623.6	4.07	2.91	4.26	8.85	22.14	0.21	0.33	0.50	0.51	0.76	0.00021
SDSS J162824.49+452811.0	0.68	0.29	0.29	0.86	1.85	0.05	0.07	0.12	0.16	0.18	
SDSS J162901.31+400759.9	11.94	1.47	2.30	5.06	14.60	0.24	0.28	0.32	0.28	0.42	0.00136
SDSS J162902.05+263845.2	22.80	0.68	1.11	3.39	6.30	0.13	0.15	0.15	0.17	0.16	
SDSS J163214.85+333412.8	13.09	0.77	0.84	1.98	4.99	0.16	0.20	0.28	0.39	0.42	0.00003
SDSS J163323.58+471859.0	65.02	4.38	5.14	27.82	76.53	0.27	0.47	0.62	0.89	0.94	0.00037
SDSS J163401.94+480940.2	7.73	0.34	0.48	1.57	4.06	0.03	0.05	0.07	0.09	0.11	0.00003
SDSS J164021.66+391306.8	1.41	0.25	0.46	1.20	3.36	0.04	0.05	0.05	0.05	0.07	
SDSS J164100.10+345452.7	2.69	2.99	3.45	12.87	28.07	0.06	0.25	0.62	1.04	1.45	
SDSS J164224.30+444509.9	2.47	1.54	2.08	4.28	12.18	0.20	0.26	0.28	0.27	0.41	0.00033
SDSS J164442.53+261913.2	90.80	1.54	2.14	5.17	12.53	0.24	0.26	0.36	0.53	0.56	0.00034
SDSS J165437.26+301654.0	7.45	0.78	0.73	1.98	2.24	0.09	0.17	0.34	0.52	0.66	
SDSS J165636.98+371439.6	5.46	0.46	0.41	0.75	2.46	0.10	0.18	0.28	0.41	0.48	0.00007
SDSS J170231.06+324719.6	1.52	13.73	17.63	29.67	63.50	1.42	1.57	1.70	2.17	2.00	0.00131
SDSS J170355.79+604511.7	3.14	0.59	0.83	2.90	5.30	0.06	0.08	0.13	0.15	0.21	0.00002
SDSS J171654.20+302701.4	3.96	1.79	3.09	5.69	9.18	0.44	0.60	0.62	0.68	0.75	
SDSS J171850.30+304201.6	0.64	2.26	3.40	8.39	21.96	0.15	0.21	0.27	0.27	0.41	0.0001
SDSS J171930.56+293412.8	1.23					0.15	0.22	0.30	0.43	0.41	0.00012
SDSS J172007.95+561710.7	2.43	0.13	0.15	0.36	1.15	0.04	0.05	0.06	0.07	0.09	0.00005
SDSS J172206.03+565451.6	39.83	0.56	0.73	2.15	6.53	0.12	0.15	0.19	0.24	0.26	0.00019
SDSS J211307.77-055541.7	2.27	3.58	3.89	15.20	24.51	0.17	0.33	0.62	1.06	1.26	
SDSS J213059.77+004438.1	3.02	0.83	0.91	1.76	4.03	0.07	0.18	0.34	0.48	0.55	
SDSS J214054.56+002538.2	0.77	6.95	8.25	16.04	37.22	0.79	1.09	1.45	2.13	2.63	0.00016
SDSS J214337.32-004724.1	2.71	0.83	1.24	2.64	5.37	0.18	0.22	0.22	0.24	0.26	
SDSS J224605.44-091925.1	0.82	1.40	1.68	3.52	9.30	0.11	0.23	0.44	0.67	0.82	
SDSS J225452.22+004631.4	0.65					0.21	0.55	0.83	1.22	1.32	
SDSS J230452.36-094413.3	1.29	0.61	0.90	3.13	9.58	0.04	0.08	0.10	0.12	0.13	
SDSS J232104.68-082537.4	5.01	0.34	0.45	1.10	4.32	0.02	0.05	0.07	0.11	0.13	
SDSS J233833.96-090039.3	1.78	2.03	3.25	8.33	22.43	0.18	0.23	0.27	0.28	0.38	
SDSS J233853.83+004812.5	9.71	0.57	0.62	2.06	3.52	0.08	0.13	0.20	0.28	0.30	
SDSS J233903.82-091221.3	4.06	3.51	5.82	11.78	25.65	0.00	0.01	0.07	0.20	0.35	
SDSS J234018.85-011027.3	11.98	0.54	0.76	1.95	6.16	0.06	0.09	0.09	0.11	0.09	
SDSS J234141.50-003806.7	0.89	1.39	1.74	4.22	12.26	0.17	0.24	0.31	0.33	0.47	0.00008
SDSS J235341.73+001801.6	1.17	0.68	1.13	2.55	6.48	0.01	0.04	0.07	0.09	0.12	

Table 2: Summary of the properties of our whole sample. In the references column Z = Zhou et al. (2006), Y = Yuan et al. (2008) and K = Komossa et al. (2006).

Source	**ref**	**RA** (°)	**Dec** (°)	z	$\mathbf{D_L}$ (Mpc)	RL	log λ**L (5100Å)** (ergs s^{-1})	**FWHM(Hβ)** (km s^{-1})	log $M_{\mathbf{BH}}$ ($M_\odot$)
SDSS J002249.22-103956.2	Z	5.7051	-10.6656	0.4139	2185	5.61	44.75	1918	7.69
SDSS J002305.04-010743.4	Z	5.771	-1.1287	0.1664	763	45.25	43.67	1214	6.60
SDSS J002752.40+002615.7	Z	6.9683	0.4377	0.2053	966	29.33	43.88	1862	7.11
SDSS J013521.68-004402.1	Z	23.8403	-0.7339	0.0985	430	3.77	43.54	1767	6.84
SDSS J014019.06-092110.5	Z	25.0794	-9.3529	0.1353	609	2.92	43.72	1576	6.86
SDSS J014644.83-004043.2	Z	26.6868	-0.6787	0.0827	358	3.92	43.47	1255	6.50
SDSS J022347.48-083655.6	Z	35.9479	-8.6154	0.2608	1272	7.86	44.01	1896	7.21
SDSS J022923.44-000047.9	Z	37.3477	-0.0133	0.5581	3132	22.70	44.67	1298	7.30
SDSS J023310.64-090940.9	Z	38.2943	-9.1614	0.388	2023	12.53	44.49	1706	7.42
SDSS J024126.71-004526.3	Z	40.3613	-0.7573	0.7254	4326	13.99	44.97	1716	7.73
SDSS J024225.87-004142.6	Z	40.6078	-0.6952	0.3827	1993	1224.46	43.58	1802	6.89
SDSS J024651.92-005931.0	Z	41.7163	-0.9919	0.4677	2533	3.37	45.21	1692	7.87
SDSS J025105.28-070230.2	Z	42.772	-7.0417	0.3268	1653	49.75	44.29	902	6.74
SDSS J025627.77-080135.0	Z	44.1157	-8.0264	0.4749	2577	56.50	44.86	1292	7.42
SDSS J030335.76+004145.0	Z	45.899	0.6958	0.6692	3916	25.75	44.87	1999	7.80
SDSS J030639.58+000343.2	Z	46.6649	0.062	0.1073	474	4.25	43.86	1904	7.11
SDSS J073256.95+320136.5	Z	113.2373	32.0268	0.6876	4058	62.04	44.2	1209	6.94
SDSS J073413.91+321722.8	Z	113.558	32.2897	0.334	1703	10.40	44.11	1613	7.13
SDSS J073953.13+310220.9	Z	114.9714	31.0392	0.3284	1670	48.89	44.36	1497	7.22
SDSS J074548.27+284838.0	Z	116.4511	28.8106	0.1584	732	3.41	43.88	1733	7.04
SDSS J074631.78+354523.7	Z	116.6324	35.7566	0.5991	3427	22.53	44.9	1979	7.81
SDSS J074636.53+430206.7	Z	116.6522	43.0352	0.5134	2840	21.71	44.45	1834	7.46
SDSS J075101.42+291419.2	Z	117.7559	29.2387	0.1208	546	1.59	44.15	1409	7.04
SDSS J075141.57+353914.8	Z	117.9232	35.6541	0.3062	1539	20.05	44.07	1896	7.24
SDSS J075209.09+414235.5	Z	118.0379	41.7099	0.2584	1265	16.16	44.09	1916	7.27
SDSS J075838.14+414512.5	Z	119.6589	41.7535	0.0935	415	4.64	43.43	1693	6.74
SDSS J080037.63+461257.9	Z	120.1568	46.2161	0.2387	1156	5.85	44.23	1538	7.16
SDSS J080203.03+435940.3	Z	120.5126	43.9945	0.0744	326	12.95	43	2061	6.63
SDSS J080306.76+302411.9	Z	120.7782	30.4033	0.3369	1721	13.34	44.07	950	6.64
SDSS J080409.24+385348.8	Z	121.0385	38.8969	0.2113	1008	9.51	44.37	1710	7.35
SDSS J080514.10+285607.2	Z	121.3088	28.9353	0.2095	999	9.80	43.7		
SDSS J080535.17+302201.7	Z	121.3965	30.3671	0.5509	3095	637.69	44.59	1114	7.11
SDSS J080710.87+245106.0	Z	121.7953	24.8517	0.3286	1672	45.10	44.07	2054	7.31
SDSS J081206.67+394017.2	Z	123.0278	39.6715	0.3785	1973	64.99	43.85	960	6.51
SDSS J081432.11+560956.6	Y	123.6338	56.1657	0.509	2812	367.93		2164	
SDSS J081516.87+460430.9	Z	123.8203	46.0753	0.0412	176	1.65	43.28	1474	6.52
SDSS J081849.27+383416.1	Z	124.7053	38.5712	0.1604	742	5.67	43.9	1067	6.64
SDSS J082007.81+372839.7	Z	125.0325	37.4777	0.0819	361	1.17	43.28	1262	6.38
SDSS J082244.88+460318.1	Z	125.687	46.055	0.3514	1807	177.36	44.2	1421	7.08
SDSS J082319.23+482516.5	Z	125.8301	48.4212	0.1489	684	6.20	43.46	1037	6.33
SDSS J082405.19+445246.1	Z	126.0216	44.8795	0.2196	1053	4.81	44.13	2014	7.33
SDSS J082433.33+380013.1	Z	126.1389	38.0037	0.1031	460	2.39	43.49	780	6.10

Continued on next page

Table 2 – *Continued from previous page*

Source	**ref**	**RA** (°)	**Dec** (°)	z	$\mathbf{D_L}$ (Mpc)	RL	$\log \lambda$**L (5100Å)** (ergs s^{-1})	**FWHM(Hβ)** (km s^{-1})	$\log M_{\mathbf{BH}}$ ($M_\odot$)
SDSS J082700.24+374822.1	Z	126.751	37.8061	0.6608	3865	5107.05	44.31	1959	7.43
SDSS J083037.75+042127.8	Z	127.6573	4.3577	0.6605	3866	17.11	44.92	2129	7.89
SDSS J083130.01+392203.6	Z	127.875	39.3677	0.2075	988	14.83	43.78	1156	6.63
SDSS J083317.45+512422.4	Z	128.3227	51.4062	0.5906	3367	5.07	44.92	1390	7.52
SDSS J083943.59+433018.0	Z	129.9316	43.505	0.1375	627	16.21	43.29	1271	6.40
SDSS J084310.79+395345.1	Z	130.795	39.8959	0.4036	2129	10.12	44.63	1650	7.48
SDSS J084610.14+445150.9	Z	131.5423	44.8641	0.6504	3791	91.76	44.58	1599	7.42
SDSS J084744.55+442610.7	Z	131.9356	44.4363	0.4652	2522	102.96	44.41	2002	7.51
SDSS J084837.66+053237.8	Z	132.1569	5.5438	0.5543	3120	10.64	44.52	1530	7.35
SDSS J084940.72+374618.3	Z	132.4197	37.7718	0.1245	564	8.25	43.38	1220	6.42
SDSS J084957.98+510829.0	Z, Y	132.4916	51.1414	0.5837	3320	4161.74	44.41	1811	7.42
SDSS J085001.17+462600.5	Z, Y	132.5049	46.4335	0.5238	2910	295.84	44.64	1251	7.25
SDSS J085152.63+522833.0	Z	132.9693	52.4758	0.0645	281	3.99	42.78	672	5.52
SDSS J085338.27+033246.1	Z	133.4095	3.5462	0.2079	992	17.61	44.1	1766	7.20
SDSS J085457.22+544820.6	Z	133.7384	54.8057	0.2559	1251	8.79	44.08	2001	7.30
SDSS J085555.53+434416.8	Z	133.9814	43.738	0.5423	3036	71.86	44.65	1609	7.47
SDSS J085613.17+363144.8	Z	134.0549	36.5291	0.1711	798	26.80	43.57	1697	6.83
SDSS J085907.58+044434.4	Z	134.7816	4.7429	0.2351	1139	14.31	43.83	1295	6.76
SDSS J090015.28+510800.2	Z	135.0637	51.1334	0.126	571	44.13	43.71	1860	7.00
SDSS J090113.23+465734.7	Z	135.3051	46.9596	0.4297	2293	21.20	44.25	1492	7.15
SDSS J090157.12+063734.6	Z	135.488	6.6263	0.5303	2957	202.59	44.22	1799	7.29
SDSS J090227.16+044309.6	Z, Y	135.6132	4.7193	0.5321	2969	1756.20	44.76	2089	7.77
SDSS J090335.47+013224.3	Z	135.8978	1.5401	0.3742	1950	9.16	44.61	1662	7.48
SDSS J090359.91+363054.7	Z	135.9996	36.5152	0.288	1435	123.26	43.79		
SDSS J090448.20+420220.0	Z	136.2008	42.0389	0.2202	1056	20.21	43.91	1031	6.61
SDSS J091146.07+403501.1	Z	137.9419	40.5837	0.4412	2368	43.13	44.46	1222	7.11
SDSS J091313.73+365817.2	Z	138.3072	36.9715	0.1073	481	16.08	43.53	1752	6.83
SDSS J091513.90+571233.2	Z	138.8079	57.2092	0.1951	921	44.77	43.34	1518	6.58
SDSS J092216.63+384448.0	Z	140.5693	38.7467	0.5897	3363	62.02	44.48	1824	7.47
SDSS J092613.80+065056.5	Z	141.5575	6.849	0.078	345	4.82	43.48	1005	6.32
SDSS J092704.38+563351.6	Z	141.7683	56.5643	0.2196	1052	92.36	43.68	2188	7.12
SDSS J092715.93+020330.7	Z	141.8164	2.0585	0.3933	2068	12.25	44.41	1828	7.43
SDSS J092856.27+013246.0	Z	142.2345	1.5461	0.2843	1416	5.99	44.09	1148	6.82
SDSS J093027.87+514141.3	Z	142.6161	51.6948	0.6239	3602	16.26	44.77	1615	7.55
SDSS J093034.79+570520.8	Z	142.645	57.0891	0.6374	3697	11.81	44.76	1567	7.52
SDSS J093048.27+404447.3	Z	142.7011	40.7465	0.1508	694	6.43	43.61	1366	6.66
SDSS J093609.14-002639.8	Z	144.0381	-0.4444	0.1411	648	2.53	43.68	1296	6.66
SDSS J094028.33+043146.1	Z	145.1181	4.5295	0.3461	1779	10.39	44.11	1622	7.13
SDSS J094121.34+011147.8	Z	145.3389	1.1966	0.4449	2396	10.79	44.62	1878	7.59
SDSS J094422.14+103739.8	Z	146.0923	10.6277	0.241	1172	7.94	44.03	1695	7.12
SDSS J094554.40+423840.0	Z	146.4767	42.6444	0.0747	328	1.03	43.5	1048	6.36
SDSS J094621.27+471131.3	Z	146.5886	47.192	0.2305	1126	7.08	44.12	1971	7.31
SDSS J094704.52+472143.0	Z	146.7688	47.362	0.5393	3015	16.07	45.01	1445	7.61

Continued on next page

Table 2 – *Continued from previous page*

Source	**ref**	**RA** (°)	**Dec** (°)	z	$\mathbf{D_L}$ (Mpc)	RL	log λ**L (5100Å)** (ergs s^{-1})	**FWHM(Hβ)** (km s^{-1})	log $M_{\mathbf{BH}}$ ($M_\odot$)
SDSS J094842.67+502931.5	Z	147.1776	50.492	0.0565	244	2.87	43.46	1800	6.81
SDSS J094857.32+002225.5	Z, Y, K	147.2388	0.3738	0.5846	3330	780.15	44.85	1432	7.50
SDSS J095257.15+050910.3	Z	148.2381	5.1529	0.5435	3048	11.87	45.2	2055	8.04
SDSS J095317.09+283601.5	Y	148.3213	28.6005	0.657	3847	613.27		2162	
SDSS J095449.94+070444.7	Z	148.7081	7.0791	0.6141	3537	18.37	44.92	1939	7.81
SDSS J095650.14+515212.2	Z	149.2089	51.8701	0.6743	3962	4.70	45.33	1879	8.04
SDSS J095823.74+011235.8	Z	149.5989	1.2099	0.5047	2786	33.69	44.42	2062	7.54
SDSS J095833.95+560224.5	Z	149.6415	56.0401	0.2164	1035	5.44	43.88	984	6.55
SDSS J095941.37+491529.5	Z	149.9224	49.2582	0.0653	285	10.75	43.2	945	6.08
SDSS J100253.51+513709.4	Z	150.723	51.6193	0.2516	1228	8.09	44.11		
SDSS J100405.00-003253.4	Z	151.0208	-0.5482	0.2886	1440	18.34	44.21	1001	6.78
SDSS J100633.91+430923.4	Z	151.6413	43.1565	0.605	3470	130.37	44.54	2175	7.66
SDSS J101435.46+433056.5	Z	153.6477	43.5157	0.5545	3120	334.11	44.51	2041	7.59
SDSS J101549.33+424243.0	Z	153.9556	42.712	0.4988	2744	24.47	44.32	2186	7.53
SDSS J101645.11+421025.5	Z	154.188	42.1737	0.0553	244	0.90	43.57	1458	6.70
SDSS J101734.76+473149.0	Z	154.3948	47.5303	0.4384	2350	23.73	44.31	2096	7.48
SDSS J101813.99+054625.5	Z	154.5583	5.7738	0.4677	2543	19.72	44.75	2160	7.79
SDSS J101936.27+002029.7	Z	154.9011	0.3416	0.1479	686	70.75	43.6	1571	6.78
SDSS J102000.45+623944.7	Z	155.0019	62.6624	0.136	619	6.28	43.43	1550	6.66
SDSS J102049.47+534539.2	Z	155.2061	53.7609	0.5837	3320	10.32	44.53	1923	7.55
SDSS J102148.90+030732.2	Z	155.4537	3.1256	0.0618	272	1.51	43.24	1686	6.61
SDSS J102256.62+540718.0	Z	155.7359	54.1217	0.3392	1734	11.02	44.14	1025	6.75
SDSS J102402.60+062943.9	Z	156.0108	6.4955	0.044	190	1.70	42.93	1564	6.35
SDSS J102531.28+514034.9	Z	156.3803	51.6764	0.0449	194	0.33	43.46	1473	6.63
SDSS J103123.73+423439.3	Y	157.8489	42.5776	0.376	1962	239.00		1642	
SDSS J103128.98+091607.2	Z	157.8708	9.2687	0.6367	3697	147.77	44.59	1719	7.49
SDSS J103210.16+065205.4	Z	158.0423	6.8682	0.0528	231	2.51	43.26		
SDSS J103352.23+521139.3	Z	158.4676	52.1943	0.5071	2799	12.00	44.82	2095	7.81
SDSS J103430.53+470820.1	Z	158.6272	47.1389	0.7798	4743	282.63	45.11	1826	7.88
SDSS J103457.29-010209.1	Z	158.7387	-1.0359	0.328	1671	15.58	44.52	1603	7.39
SDSS J103615.68+031916.7	Z	159.0653	3.3213	0.3893	2043	6.33	44.44	1688	7.38
SDSS J103727.45+003635.6	Z, Y	159.3644	0.6099	0.5952	3405	545.65	44.51	1357	7.24
SDSS J104541.76+520235.5	Z	161.424	52.0432	0.2839	1411	1.81	44.76	1589	7.53
SDSS J104732.68+472532.1	Z, Y	161.8861	47.4256	0.7982	4882	10345.74	44.94	2153	7.91
SDSS J104808.25+551954.7	Z	162.0344	55.3319	0.4269	2276	10.16	44.27	1136	6.93
SDSS J105547.44+492950.8	Z	163.9477	49.4975	0.6253	3612	29.66	44.73	2086	7.75
SDSS J105558.16+552310.4	Z	163.9923	55.3862	0.4657	2525	26.20	44.37	1604	7.29
SDSS J110333.01+083449.0	Z	165.8875	8.5803	0.1631	759	10.35	43.69	1151	6.57
SDSS J110423.64+503404.3	Z	166.0985	50.5679	0.1253	567	5.93	43.46	1227	6.48
SDSS J110542.72+020250.9	Z	166.428	2.0475	0.4547	2458	2012.34	44.4	1256	7.10
SDSS J110703.76+004202.3	Z	166.7657	0.7006	0.5799	3295	17.74	44.78	2120	7.80
SDSS J110747.83+013933.5	Z	166.9493	1.6593	0.7365	4423	22.15	44.48	2144	7.61
SDSS J110931.25+632623.4	Z	167.3802	63.4398	0.4568	2467	22.92	44.49	1583	7.36

Continued on next page

Table 2 – *Continued from previous page*

Source	**ref**	**RA** (°)	**Dec** (°)	z	$\mathbf{D_L}$ (Mpc)	RL	$\log \lambda\mathbf{L}$ **(5100Å)** (ergs s^{-1})	**FWHM(Hβ)** (km s^{-1})	$\log M_{\mathbf{BH}}$ ($M_\odot$)
SDSS J111005.03+365336.3	Y	167.521	36.8934	0.63	3651	1251.14		1300	
SDSS J111340.41+040211.2	Z	168.4184	4.0365	0.4471	2409	20.73	44.24	1269	7.00
SDSS J111450.07+502917.2	Z	168.7086	50.4881	0.4512	2432	95.81	44.27	1004	6.82
SDSS J111756.86-000220.6	Z	169.4869	-0.039	0.4569	2472	215.11	44.15	1724	7.21
SDSS J111934.01+533518.7	Z	169.8917	53.5885	0.106	474	25.87	43.77	562	6.00
SDSS J112016.17+491428.8	Z	170.0674	49.2413	0.1496	688	176.45	43.39	1525	6.62
SDSS J112042.75+084131.2	Z	170.1781	8.692	0.2753	1365	6.77	44.2	1002	6.77
SDSS J112108.59+535121.1	Z	170.2858	53.8559	0.1029	459	2.63	44.26	2105	7.46
SDSS J112114.22+032546.8	Z	170.3093	3.4297	0.152	703	4.09	44.06	1981	7.28
SDSS J112444.54+040927.1	Z	171.1856	4.1575	0.2496	1220	18.70	43.95	1108	6.70
SDSS J112521.60+052358.2	Z	171.34	5.3995	0.4218	2247	441.55	44.26	1028	6.83
SDSS J112702.72+030152.0	Z	171.7613	3.0311	0.416	2211	122.63	44.35	1991	7.47
SDSS J112813.03+102308.3	Z	172.0543	10.3856	0.0504	221	0.87	43.42	1184	6.42
SDSS J112941.94+512050.7	Z	172.4247	51.3474	0.2338	1130	2.92	44.39	1396	7.18
SDSS J113001.89+494434.8	Z	172.5079	49.743	0.2443	1188	2.95	44.28	2117	7.47
SDSS J113055.88+024800.0	Z	172.7328	2.8	0.2976	1493	50.37	43.92	1240	6.78
SDSS J113320.91+043255.2	Z	173.3371	4.5487	0.2481	1212	24.49	44.14	2184	7.41
SDSS J113427.09+100113.0	Z	173.6129	10.0203	0.5256	2926	18.86	44.86	2192	7.88
SDSS J113452.07+563723.9	Z	173.717	56.6233	0.254	1241	21.52	43.79	992	6.50
SDSS J113625.42+100523.2	Z	174.1059	10.0898	0.5526	3110	5.38	45.09	1602	7.75
SDSS J113824.54+365327.1	Y	174.6023	36.8908	0.356	1839	271.74		1364	
SDSS J114256.64+042731.4	Z	175.736	4.4587	0.4375	2347	3.83	44.67	1897	7.63
SDSS J114654.28+323652.3	Y	176.7262	32.6145	0.465	2523	140.37		2081	
SDSS J114805.31-023303.6	Z	177.0221	-2.551	0.5657	3200	15.66	45.05	2175	7.99
SDSS J114954.99+044812.9	Z	177.4791	4.8036	0.2695	1332	4.10	44.5	1631	7.39
SDSS J115215.84+042456.2	Z	178.066	4.4156	0.1327	606	14.22	43.29	1783	6.69
SDSS J115507.61+520129.6	Z	178.7817	52.0249	0.154	710	3.15	44.06	1130	6.79
SDSS J115544.40+040631.6	Z	178.935	4.1088	0.1686	787	2.33	43.87	1342	6.82
SDSS J115636.54+020827.1	Z	179.1522	2.1409	0.4845	2653	29.45	44.52	1582	7.37
SDSS J115637.77+051633.6	Z	179.1574	5.276	0.3971	2092	34.69	44.2	1200	6.93
SDSS J115644.79+110228.1	Z	179.1866	11.0412	0.5189	2881	25.14	44.33	1704	7.32
SDSS J115753.20-031537.1	Z	179.4717	-3.2603	0.2146	1025	8.45	44.25	1480	7.14
SDSS J120014.08-004638.7	Z	180.0587	-0.7774	0.1794	843	73.10	43.92	1945	7.17
SDSS J120113.77-024241.3	Z	180.3074	-2.7115	0.3072	1548	21.28	44.01	1486	6.99
SDSS J120226.76-012915.3	Z	180.6115	-1.4876	0.1502	696	19.88	44.02	1118	6.75
SDSS J120628.98+503001.5	Z	181.6207	50.5004	0.172	802	8.52	43.57	1479	6.71
SDSS J120652.44+515918.7	Z	181.7185	51.9885	0.3984	2096	16.91	44.2	1739	7.25
SDSS J120700.30-021927.2	Z	181.7513	-2.3242	0.3085	1556	17.23	44.23	906	6.70
SDSS J120806.90-013509.7	Z	182.0288	-1.586	0.4805	2627	25.73	44.36	1763	7.37
SDSS J121325.48+092319.5	Z	183.3562	9.3887	0.7239	4330	16.11	45.04	1460	7.64
SDSS J121549.44+544224.0	Z	183.956	54.7067	0.15	691	3.07	44.2	984	6.76
SDSS J121845.55-012545.8	Z	184.6898	-1.4294	0.2387	1160	44.97	43.9	1319	6.82
SDSS J122102.95-000733.8	Z	185.2623	-0.126	0.3662	1902	6.44	44.38	848	6.74

Continued on next page

Table 2 – *Continued from previous page*

Source	**ref**	**RA** (°)	**Dec** (°)	z	$\mathbf{D_L}$ (Mpc)	RL	log λ**L (5100Å)** (ergs s^{-1})	**FWHM(Hβ)** (km s^{-1})	log $M_{\mathbf{BH}}$ ($M_\odot$)
SDSS J122753.10+024215.8	Z	186.9713	2.7044	0.3118	1575	38.77	44.1	1605	7.12
SDSS J123417.88+102543.0	Z	188.5745	10.4286	0.3551	1833	15.03	44.57	1765	7.50
SDSS J123852.12+394227.8	Y	189.7173	39.7077	0.622	3595	252.16		910	
SDSS J124634.65+023809.0	Z, Y	191.6444	2.6358	0.3627	1879	243.20	44.43	1425	7.23
SDSS J124635.25+022208.8	Z	191.6469	2.3691	0.0482	210	1.44	43.49	811	6.14
SDSS J125051.05+060910.0	Z	192.7127	6.1528	0.182	856	6.02	44.13	1921	7.29
SDSS J125337.36-004809.6	Z	193.4057	-0.8027	0.4268	2278	4.56	44.4	1424	7.21
SDSS J125635.89+500852.4	Z	194.1495	50.1479	0.2453	1193	3203.14	43.66	1806	6.94
SDSS J130034.40+501112.8	Z	195.1433	50.1869	0.7093	4218	19.82	44.66	2113	7.72
SDSS J130052.11+564105.9	Z	195.2171	56.685	0.0718	314	42.94	43.4	1973	6.85
SDSS J130522.75+511640.3	Z, Y	196.3448	51.2779	0.7853	4783	249.70	45.55	1925	8.20
SDSS J130916.67-001550.2	Z	197.3195	-0.2639	0.4222	2252	12.63	44.12	1028	6.74
SDSS J131136.36+580801.6	Z	197.9015	58.1338	0.0711	310	8.42	43.15	2058	6.73
SDSS J132206.76+561213.0	Z	200.5282	56.2036	0.6214	3583	32.21	44.83	1414	7.48
SDSS J132447.10+530257.7	Z	201.1962	53.0494	0.292	1456	697.22	43.89	1917	7.14
SDSS J132832.51-010318.0	Z	202.1355	-1.055	0.7366	4426	27.46	44.8	1806	7.67
SDSS J133138.04+013151.7	Z	202.9085	1.531	0.0805	356	7.44	43.41	1763	6.76
SDSS J133450.44+010218.8	Z	203.7102	1.0386	0.2453	1195	14.01	44.07	1196	6.84
SDSS J133619.63+540150.9	Z	204.0818	54.0308	0.481	2625	26.23	44.36	1955	7.46
SDSS J133724.33+600541.7	Z	204.3514	60.0949	0.2339	1129	32.12	43.95	961	6.58
SDSS J133757.03+565631.3	Z	204.4876	56.942	0.3711	1926	7.62	44.19	1620	7.18
SDSS J133819.96-025250.8	Z	204.5832	-2.8808	0.5782	3285	75.81	44.64	1909	7.61
SDSS J134206.57+050523.9	Z	205.5274	5.09	0.266	1311	7.16	44.56	1786	7.51
SDSS J134426.42+441620.1	Z	206.1101	44.2722	0.0547	237	5.11	43.23	1248	6.34
SDSS J135121.43+481355.8	Z	207.8393	48.2322	0.7393	4439	23.90	44.66	1575	7.46
SDSS J135516.55+561244.7	Z	208.819	56.2124	0.1217	549	8.86	44.01	1127	6.75
SDSS J135618.50-011514.0	Z	209.0771	-1.2539	0.2473	1206	54.58	43.7	1178	6.59
SDSS J135908.01+002731.9	Z	209.7834	0.4589	0.2569	1258	19.50	44.01	1266	6.85
SDSS J140130.81+570453.2	Z	210.3784	57.0815	0.4147	2197	8.61	44.5	1722	7.44
SDSS J140322.11+022232.9	Z	210.8421	2.3758	0.2502	1222	75.12	43.65	1456	6.75
SDSS J140914.36+565625.7	Z	212.3098	56.9405	0.2386	1155	29.90	44.12	1581	7.12
SDSS J141049.55+015135.0	Z	212.7065	1.8597	0.2009	954	13.85	43.75	1495	6.83
SDSS J141700.54+415219.2	Z	214.2523	41.872	0.6322	3660	10.06	44.72	1197	7.26
SDSS J142033.71+573901.0	Z	215.1404	57.6503	0.7361	4414	124.86	45.15	1904	7.94
SDSS J142441.21-000727.2	Z	216.1717	-0.1242	0.3183	1610	18.82	44.27	1183	6.96
SDSS J142830.17+555931.3	Z	217.1257	55.992	0.3514	1806	81.79	44.13	2121	7.38
SDSS J143249.69+451338.3	Z	218.2071	45.2273	0.3069	1542	24.89	44.06	1844	7.21
SDSS J143453.83+592626.4	Z	218.7243	59.4407	0.7713	4676	9.17	45.08	1858	7.87
SDSS J143509.49+313147.8	Y	218.7897	31.5301	0.501	2763	855.37		1719	
SDSS J143701.20-010418.1	Z	219.255	-1.0717	0.2858	1422	33.69	44.11	1659	7.15
SDSS J143952.92+392359.0	Z	219.9705	39.3997	0.112	502	6.30	43.35	1530	6.60
SDSS J144012.76+615633.2	Z	220.0532	61.9425	0.2755	1360	5.13	44.66	1633	7.49
SDSS J144043.34+613008.8	Z	220.1806	61.5024	0.4423	2372	12.84	44.34	1135	6.97

Continued on next page

Table 2 – *Continued from previous page*

Source	**ref**	**RA** (°)	**Dec** (°)	z	$\mathbf{D_L}$ (Mpc)	RL	log λ**L (5100Å)** (ergs s^{-1})	**FWHM(Hβ)** (km s^{-1})	log $M_{\mathbf{BH}}$ ($M_\odot$)
SDSS J144303.81+035749.8	Z	220.7659	3.9638	0.1131	509	11.14	43.06	1160	6.17
SDSS J144318.56+472556.7	Y	220.8274	47.4323	0.703	4172	1016.70		1848	
SDSS J144751.79+505328.8	Z	221.9658	50.8913	0.3057	1535	10.11	44.16	1527	7.11
SDSS J144848.67+372935.7	Z	222.2028	37.4933	0.243	1180	599.33	43.7	1331	6.70
SDSS J144855.21+575503.5	Z	222.2301	57.9176	0.6517	3797	17.02	44.64	1283	7.27
SDSS J144903.19+503018.2	Z	222.2633	50.5051	0.6083	3490	10.28	44.55	1910	7.56
SDSS J145041.93+591936.9	Z	222.6747	59.3269	0.202	956	22.50	43.79	1159	6.64
SDSS J145751.91+000011.5	Z	224.4663	0.0032	0.1872	881	42.16	43.59	1085	6.45
SDSS J150225.27+490220.7	Z	225.6053	49.0391	0.1223	551	3.42	43.31	819	6.03
SDSS J150506.48+032630.8	Z, Y	226.277	3.4419	0.4089	2162	2924.08	44.36	1082	6.94
SDSS J150521.92+014149.8	Z	226.3413	1.6972	0.1579	730	5.56	43.84	1125	6.64
SDSS J150734.51+403627.9	Z	226.8938	40.6078	0.2517	1227	8.16	43.66	1237	6.61
SDSS J150832.91+583422.5	Z	227.1371	58.5729	0.5022	2763	158.67	44.06	2050	7.31
SDSS J151131.33+502219.0	Z	227.8805	50.3719	0.2198	1052	14.32	44.01	2108	7.30
SDSS J151617.16+472805.1	Z	229.0715	47.4681	0.1979	935	163.19	43.61	1657	6.83
SBS1517+520	K	229.6369	51.9158	0.371	1926	28.49			
SDSS J152205.41+393441.3	Z	230.5225	39.5781	0.0766	335	2.05	43.27	787	5.97
SDSS J152429.34+351522.1	Z	231.1223	35.2561	0.2494	1215	32.94	44.04	1053	6.71
SDSS J152628.19-003809.5	Z	231.6175	-0.636	0.1233	558	3.53	43.76	2139	7.15
SDSS J152829.40+033027.7	Z	232.1225	3.5077	0.3256	1653	24.02	43.98	1339	6.88
SDSS J153243.67-004342.5	Z	233.182	-0.7285	0.3089	1552	54.26	43.95		
SDSS J153705.95+005522.8	Z	234.2748	0.923	0.1364	621	1.50	44.08	1926	7.26
SDSS J153732.62+494247.7	Z	234.3859	49.7133	0.2797	1384	10.94	44.23	1134	6.90
SDSS J153903.95+571605.9	Z	234.7665	57.2683	0.4965	2725	24.94	44.24	1592	7.20
SDSS J153911.16+002600.7	Z	234.7965	0.4335	0.2648	1301	5.30	44.18	1184	6.91
SDSS J154530.24+484609.1	Z	236.376	48.7692	0.3996	2101	2.28	45.25	1821	7.96
SDSS J154653.02+571013.7	Z	236.7209	57.1705	0.438	2343	7.92	44.53	1583	7.38
SDSS J154817.92+351128.0	Y	237.0747	35.1911	0.478	2608	677.22		2035	
SDSS J154830.89+563012.1	Z	237.1287	56.5034	0.6933	4097	22.93	44.83	1557	7.56
SDSS J155433.22+453646.4	Z	238.6384	45.6129	0.517	2862	23.02	44.51	1177	7.11
SDSS J155451.14+461917.4	Z	238.7131	46.3215	0.1169	524	4.45	43.43	1541	6.65
SDSS J155609.81+030922.3	Z	239.0409	3.1562	0.1307	593	1.10	44.15	1102	6.82
SDSS J155936.14+544203.9	Z	239.9006	54.7011	0.3077	1545	27.85	44.2	1924	7.34
SDSS J160404.53+493820.5	Z	241.0189	49.639	0.1486	680	47.43	42.99	1827	6.52
SDSS J160424.17+271759.1	Z	241.1007	27.2998	0.7794	4736	11.97	44.93	2120	7.89
SDSS J160452.44+473320.1	Z	241.2185	47.5556	0.7365	4415	8.90	44.76	1850	7.66
SDSS J160518.50+375653.4	Z	241.3271	37.9482	0.2009	950	256.85	44.23	1913	7.35
SDSS J160558.12+440319.5	Z	241.4921	44.0555	0.0444	190	1.50	43.02	2124	6.67
SDSS J161301.87+524749.6	Z	243.2578	52.7971	0.5279	2935	12.69	44.59	1382	7.30
SDSS J162012.76+400906.2	Z	245.0532	40.1517	0.0285	121	0.35	42.77	1240	6.04
SDSS J162348.97+392503.5	Z	245.954	39.4176	0.6967	4122	91.84	44.76	1415	7.43
SDSS J162458.42+423107.5	Z	246.2434	42.5188	0.6633	3879	29.90	44.93	1437	7.55
SDSS J162543.14+490059.0	Z	246.4298	49.0164	0.5449	3049	133.25	44.29	1725	7.30

Continued on next page

Table 2 – *Continued from previous page*

Source	**ref**	**RA** (°)	**Dec** (°)	z	$\mathbf{D_L}$ (Mpc)	RL	log λ**L (5100Å)** (ergs s^{-1})	**FWHM(Hβ)** (km s^{-1})	log $M_{\mathbf{BH}}$ ($M_\odot$)
SDSS J162611.87+372536.2	Z	246.5495	37.4267	0.6303	3644	6.95	44.8	1364	7.43
SDSS J162750.56+473623.6	Z	246.9607	47.6066	0.2624	1283	13.29	44.61	1996	7.63
SDSS J162824.49+452811.0	Z	247.1021	45.4697	0.2279	1095	10.23	43.63	866	6.28
SDSS J162901.31+400759.9	Z, K	247.2555	40.1333	0.2719	1339	45.30	44.31	1238	7.03
SDSS J162902.05+263845.2	Z	247.2585	26.6459	0.6282	3629	163.72	44.81	1467	7.49
SDSS J163214.85+333412.8	Z	248.0619	33.5702	0.1741	810	65.83	43.84	2092	7.18
SDSS J163323.58+471859.0	Z, Y	248.3483	47.3164	0.1161	520	143.96	43.81	909	6.44
SDSS J163401.94+480940.2	Z, Y	248.5081	48.1612	0.4948	2713	168.88	44.38	1609	7.30
SDSS J164021.66+391306.8	Z	250.0902	39.2185	0.345	1766	31.40	43.77	732	6.23
SDSS J164100.10+345452.7	Z	250.2504	34.9146	0.1641	758	13.08	43.81	2071	7.15
SDSS J164224.30+444509.9	Z	250.6013	44.7527	0.3684	1907	10.65	44.47	1735	7.42
SDSS J164442.53+261913.2	Y	251.1772	26.3204	0.144	662	320.29		1507	
SDSS J165437.26+301654.0	Z	253.6553	30.2817	0.1857	869	44.45	43.65	1616	6.84
SDSS J165636.98+371439.6	Z	254.1541	37.2443	0.0628	270	30.75	42.72	1742	6.31
SDSS J170231.06+324719.6	Z	255.6294	32.7888	0.1633	754	0.92	44.64	1694	7.51
SDSS J170355.79+604511.7	Z	255.9825	60.7533	0.2847	1411	39.90	44.04	1377	6.95
SDSS J171654.20+302701.4	Z	259.2258	30.4504	0.7537	4541	7.72	45.64	2190	8.37
SDSS J171850.30+304201.6	Z	259.7096	30.7005	0.2818	1394	3.01	44.33	1309	7.09
SDSS J171930.56+293412.8	Z	259.8774	29.5702	0.1804	841	5.49	43.89	983	6.56
SDSS J172007.95+561710.7	Z	260.0331	56.2863	0.3888	2033	49.51	43.96	1206	6.78
SDSS J172206.03+565451.6	Z, Y, K	260.5251	56.9143	0.4253	2263	285.14	44.55	1385	7.28
SDSS J211307.77-055541.7	Z	318.2824	-5.9282	0.1303	584	6.40	43.74	1265	6.68
SDSS J213059.77+004438.1	Z	322.749	0.7439	0.1301	582	17.51	43.65	1496	6.77
SDSS J214054.56+002538.2	Z	325.2273	0.4273	0.0838	362	0.64	43.87	1652	7.00
SDSS J214337.32-004724.1	Z	325.9055	-0.79	0.4463	2389	13.36	44.69	1910	7.65
SDSS J224605.44-091925.1	Z	341.5227	-9.3236	0.1185	525	3.49	43.34	1722	6.69
SDSS J225452.22+004631.4	Z	343.7176	0.7754	0.0907	393	1.22	43.71	1508	6.81
SDSS J230452.36-094413.3	Z	346.2182	-9.737	0.6902	4065	19.87	44.75	1282	7.34
SDSS J232104.68-082537.4	Z	350.2695	-8.427	0.4512	2420	118.76	44.31	1355	7.11
SDSS J233833.96-090039.3	Z	354.6415	-9.0109	0.374	1934	8.06	44.56	2060	7.63
SDSS J233853.83+004812.5	Z	354.7243	0.8035	0.1697	781	79.77	43.55	1061	6.41
SDSS J233903.82-091221.3	Z	354.7659	-9.2059	0.6604	3850	428.72	45.13	1950	7.95
SDSS J234018.85-011027.3	Z	355.0786	-1.1743	0.5512	3085	161.36	44.47	1822	7.47
SDSS J234141.50-003806.7	Z	355.4229	-0.6352	0.3193	1605	4.07	44.54	1736	7.47
SDSS J235341.73+001801.6	Z	358.4239	0.3005	0.7522	4519	42.11	44.88	1387	7.49

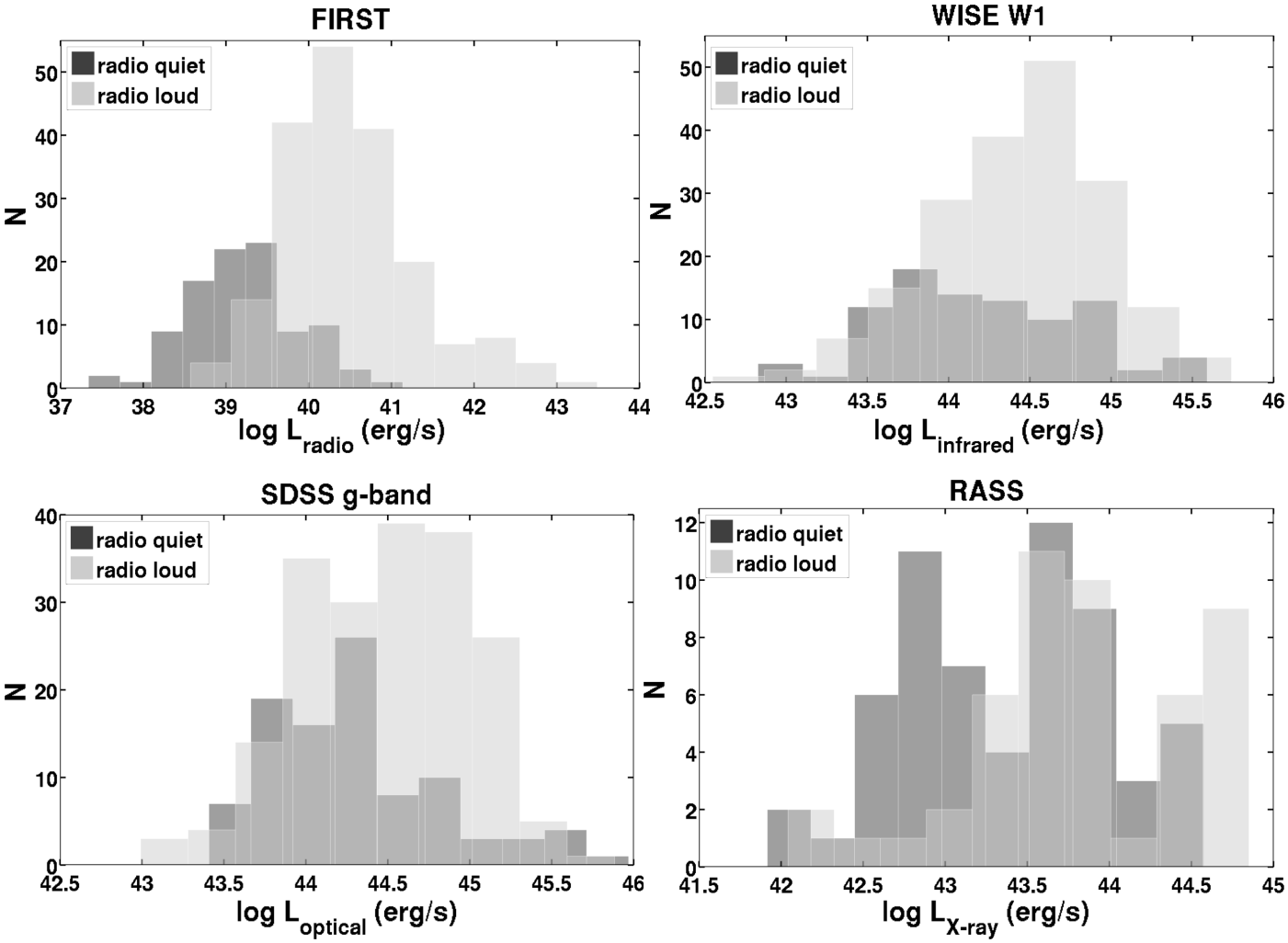

Fig. 2: Luminosity distributions of the radio-quiet and radio-loud subsamples for the wavebands for which we present the correlation results; FIRST, WISE W1-band, SDSS *g*-band and RASS.

Table 5: Pearson's r and Spearman's ρ flux density correlations and their p-values for the whole sample and the subsamples. Correlations in boldface have p<0.05

	$\log F_O$ - $\log F_R$		$\log F_O$ - $\log F_{IR}$		$\log F_O$ - $\log F_X$	
sample	Pearson's r (p)	Spearman's ρ (p)	r (p)	ρ (p)	r (p)	ρ (p)
all	-0.024 (0.678)	0.053 (0.363)	**0.810** ($\sim 10^{-67}$)	**0.787** ($\sim 10^{-61}$)	**0.556** ($\sim 10^{-10}$)	**0.548** ($\sim 10^{-10}$)
RQ	**0.645** ($\sim 10^{-13}$)	**0.658** (~0)	**0.840** ($\sim 10^{-25}$)	**0.843** ($\sim 10^{-25}$)	**0.592** ($\sim 10^{-7}$)	**0.597** ($\sim 10^{-7}$)
RL	**0.248** ($\sim 10^{-4}$)	**0.304** ($\sim 10^{-5}$)	**0.630** ($\sim 10^{-22}$)	**0.601** ($\sim 10^{-20}$)	**0.456** (0.001)	**0.484** ($\sim 10^{-4}$)
VRL	**0.560** ($\sim 10^{-5}$)	**0.609** ($\sim 10^{-6}$)	**0.509** ($\sim 10^{-4}$)	**0.581** ($\sim 10^{-6}$)	**0.627** (0.009)	**0.579** (0.021)
SRL	**0.744** (0.014)	0.467 (0.178)	**0.918** ($\sim 10^{-4}$)	**0.855** (0.004)	0.115 (0.885)	-0.200 (0.917)

	$\log F_R$ - $\log F_{IR}$		$\log F_R$ - $\log F_X$	
sample	Pearson's r (p)	Spearman's ρ (p)	r (p)	ρ (p)
all	-0.055 (0.360)	-0.017 (0.782)	0.047 (0.624)	0.130 (0.179)
RQ	**0.548** ($\sim 10^{-8}$)	**0.571** ($\sim 10^{-9}$)	0.251 (0.053)	**0.333** (0.010)
RL	0.131 (0.071)	**0.142** (0.049)	0.213 (0.141)	0.255 (0.077)
VRL	0.181 (0.202)	**0.289** (0.039)	0.229 (0.394)	0.159 (0.556)
SRL	**0.687** (0.028)	0.418 (0.232)	-0.205 (0.795)	0.200 (0.917)

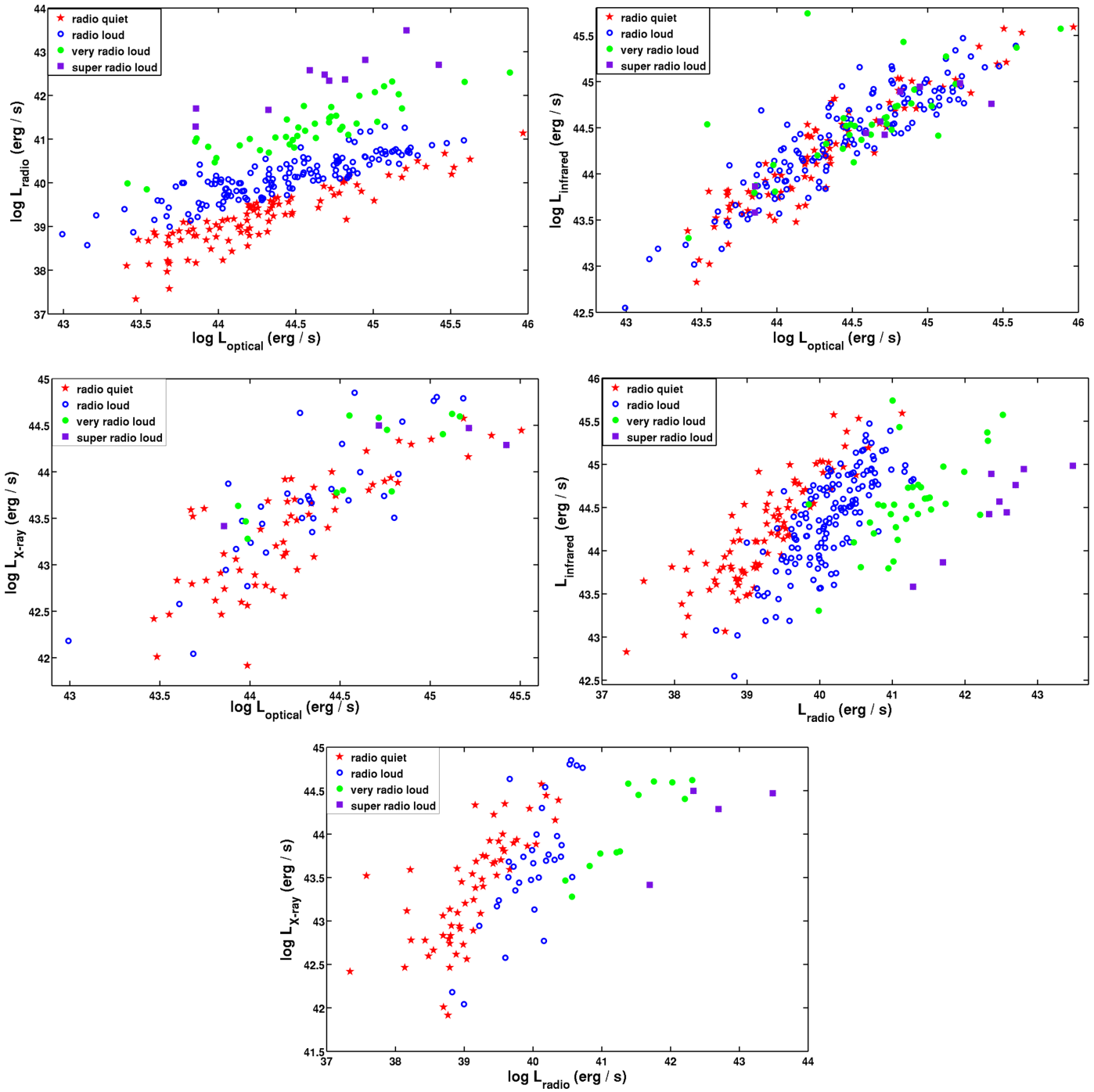

Fig. 4: Luminosity dependencies between the wavebands we used to compute the correlations. Subsamples are shown with different symbols and colors; radio-quiet: filled red stars, radio-loud: open blue circles, very radio-loud: filled green circles, and super radio-loud: filled purple squares.

Table 7: Linear fits of the flux densities for the radio-quiet and radio-loud subsamples.

RADIO QUIET SAMPLE
$\log S_{O} = 0.994(\pm0.012)\log S_{R}$ - $0.604(\pm0.034)$
$\log S_{IR} = 0.759(\pm0.013)\log S_{R}$ - $0.447(\pm0.039)$
$\log S_{X} = 0.344(\pm0.018)\log S_{R}$ - $5.808(\pm0.051)$
$\log S_{IR} = 0.753(\pm0.013)\log S_{O}$ - $0.013(\pm0.047)$
$\log S_{X} = 0.568(\pm0.015)\log S_{O}$ - $4.863(\pm0.051)$
$\log S_{X} = 0.648(\pm0.018)\log S_{IR}$ - $5.119(\pm0.046)$

RADIO LOUD SAMPLE
$\log S_{O} = 0.132(\pm0.002)\log S_{R}$ - $3.820(\pm0.005)$
$\log S_{IR} = 0.070(\pm0.002)\log S_{R}$ - $2.984(\pm0.005)$
$\log S_{X} = 0.119(\pm0.010)\log S_{R}$ - $6.729(\pm0.023)$
$\log S_{IR} = 0.638(\pm0.004)\log S_{O}$ - $0.513(\pm0.018)$
$\log S_{X} = 0.546(\pm0.024)\log S_{OP}$ - $4.836(\pm0.094)$
$\log S_{X} = 0.311(\pm0.019)\log S_{IR}$ - $6.046(\pm0.057)$

Table 8: Linear fits of the luminosities for the radio-quiet and radio-loud subsamples.

RADIO QUIET SAMPLE
$\log L_{O} = 0.705(\pm0.006)\log L_{R}$ + $16.654(\pm0.249)$
$\log L_{IR} = 0.754(\pm0.006)\log L_{R}$ + $14.629(\pm0.226)$
$\log L_{X} = 0.754(\pm0.008)\log L_{R}$ + $13.882(\pm0.328)$
$\log L_{IR} = 1.012(\pm0.010)\log L_{O}$ - $0.562(\pm0.425)$
$\log L_{X} = 1.107(\pm0.013)\log L_{O}$ - $5.606(\pm0.572)$
$\log L_{X} = 0.908(\pm0.011)\log L_{IR}$ + $3.308(\pm0.504)$

RADIO LOUD SAMPLE
$\log L_{O} = 0.404(\pm0.001)\log L_{R}$ + $28.118(\pm0.046)$
$\log L_{IR} = 0.373(\pm0.001)\log L_{R}$ + $29.325(\pm0.042)$
$\log L_{X} = 0.419(\pm0.006)\log L_{R}$ + $26.810(\pm0.235)$
$\log L_{IR} = 0.915(\pm0.003)\log L_{O}$ + $3.710(\pm0.126)$
$\log L_{X} = 1.121(\pm0.016)\log L_{O}$ - $5.964(\pm0.719)$
$\log L_{X} = 0.924(\pm0.012)\log L_{IR}$ + $2.841(\pm0.554)$

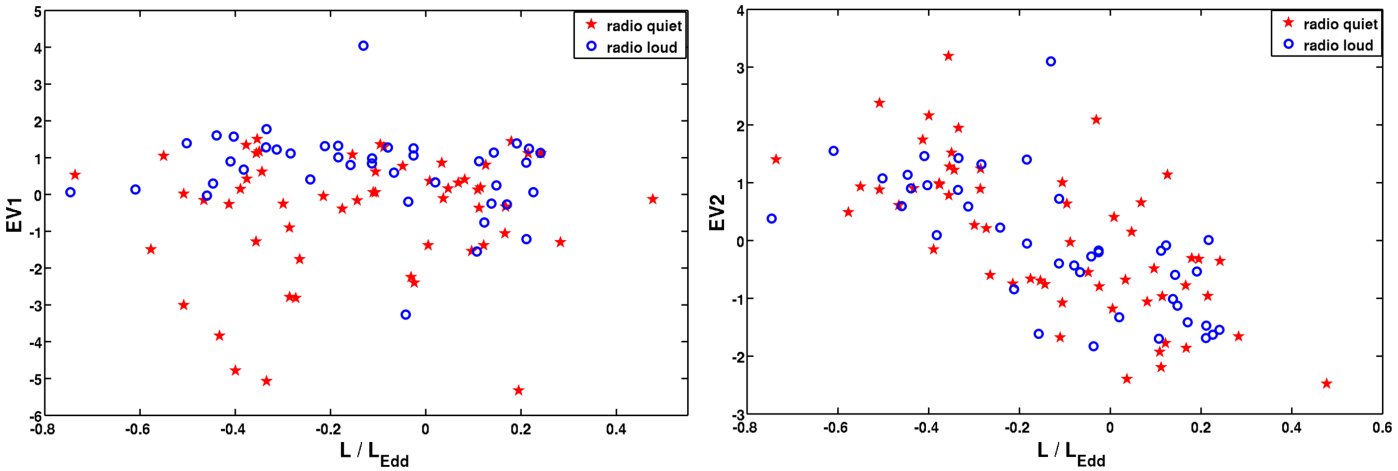

Fig. 5: Dependency between the Eddington ratio and Eigenvectors 1 and 2 from the PCA with seven variables. Radio-loud and radio-quiet subsamples are shown with different symbols and colors; radio-quiet: filled red stars, and radio-loud: open blue circles.

Table 12: $M_{\rm BH}$ – luminosity correlations for the whole sample and the subsamples. The upper value is Pearson's r and the lower value is Spearman's ρ (p-value in parentheses). Correlations in boldface have p<0.05

		$\log M_{\rm BH} - \log L_{\rm R}$	$\log M_{\rm BH} - \log L_{\rm O}$	$\log M_{\rm BH} - \log L_{\rm IR}$	$\log M_{\rm BH} - \log L_{\rm X}$
All	r (p)	**0.632** ($\sim 10^{-32}$)	**0.836** ($\sim 10^{-73}$)	**0.831** ($\sim 10^{-69}$)	**0.683** ($\sim 10^{-15}$)
	ρ (p)	**0.673** ($\sim$0)	**0.857** ($\sim$0)	**0.840** ($\sim$0)	**0.711** ($\sim$0)
RQ	r (p)	**0.790** ($\sim 10^{-21}$)	**0.843** ($\sim 10^{-26}$)	**0.890** ($\sim 10^{-30}$)	**0.679** ($\sim 10^{-9}$)
	ρ (p)	**0.793** ($\sim$0)	**0.848** ($\sim$0)	**0.894** ($\sim$0)	**0.716** ($\sim$0)
RL	r (p)	**0.580** ($\sim 10^{-17}$)	**0.823** ($\sim 10^{-46}$)	**0.788** ($\sim 10^{-39}$)	**0.669** ($\sim 10^{-6}$)
	ρ (p)	**0.634** ($\sim$0)	**0.836** ($\sim$0)	**0.803** ($\sim$0)	**0.647** ($\sim 10^{-6}$)
VRL	r (p)	**0.470** (0.003)	**0.748** ($\sim 10^{-8}$)	**0.832** ($\sim 10^{-11}$)	**0.704** (0.034)
	ρ (p)	**0.351** (0.029)	**0.671** ($\sim 10^{-6}$)	**0.803** ($\sim 10^{-8}$)	**0.700** (0.043)
SRL	r (p)	**0.768** (0.026)	**0.769** (0.026)	**0.794** (0.019)	0.608 (0.584)
	ρ (p)	**0.786** (0.028)	**0.810** (0.022)	**0.833** (0.015)	0.500 (1.000)

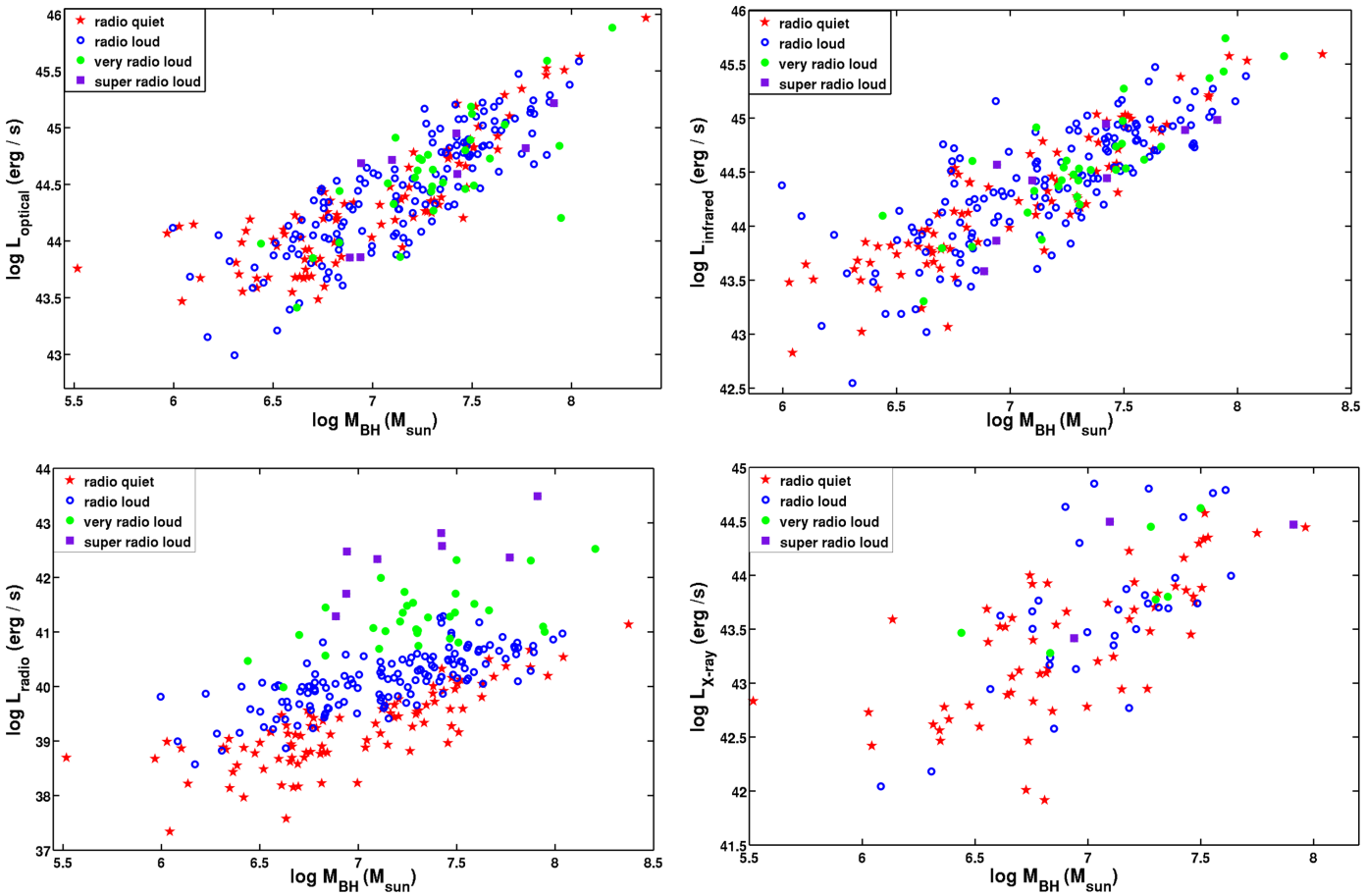

Fig. 7: Dependencies between the black hole mass and luminosities. Subsamples are shown with different symbols and colors; radio-quiet: filled red stars, radio-loud: open blue circles, very radio-loud: filled green circles, and super radio-loud: filled purple squares.

Table 13: FWHM(Hβ) – luminosity correlations for the whole sample and the subsamples. The upper value is Pearson's r and the lower value is Spearman's ρ (p-value in parentheses). Correlations in boldface have p<0.05

		FWHM – log L_R	FWHM – log L_O	FWHM – log L_{IR}	FWHM – log L_X
All	r (p)	**0.264** ($\sim 10^{-5}$)	**0.305** ($\sim 10^{-7}$)	**0.282** ($\sim 10^{-6}$)	0.024 (0.808)
	ρ (p)	**0.287** ($\sim 10^{-6}$)	**0.302** ($\sim 10^{-7}$)	**0.298** ($\sim 10^{-7}$)	0.045 (0.655)
RQ	r (p)	**0.312** (0.002)	**0.323** (0.001)	**0.361** ($\sim 10^{-4}$)	0.059 (0.653)
	ρ (p)	**0.303** (0.003)	**0.312** (0.002)	**0.369** ($\sim 10^{-4}$)	0.094 (0.476)
RL	r (p)	**0.242** (0.001)	**0.281** ($\sim 10^{-4}$)	**0.233** (0.002)	-0.099 (0.536)
	ρ (p)	**0.282** ($\sim 10^{-4}$)	**0.290** ($\sim 10^{-5}$)	**0.263** ($\sim 10^{-4}$)	-0.083 (0.604)
VRL	r (p)	0.111 (0.500)	0.159 (0.333)	0.210 (0.199)	0.015 (0.970)
	ρ (p)	0.056 (0.735)	0.162 (0.322)	0.263 (0.105)	-0.150 (0.708)
SRL	r (p)	0.209 (0.620)	0.111 (0.793)	0.182 (0.666)	-0.151 (0.903)
	ρ (p)	0.578 (0.171)	0.524 (0.197)	0.595 (0.132)	-0.500 (1.000)